(2)

AFOSR-TR- 91 0120

Annual Technical Report
for
AFOSR Grant No. 89-0201

HIGH TEMPERATURE DEFORMATION PROCESSES AND STRENGTHENING MECHANISMS IN INTERMETALLIC PARTICULATE COMPOSITES

Submitted to :

Department of the Air Force
Directorate of Electronic and Materials Sciences
Air Force of Office of Scientific Research
Bolling Air Force Base, Building 410
Washington D.C. 20332

Attention: Dr. Alan Rosenstein

Submitted by:

Professor William D. Nix, Principal Investigator
Department of Materials Science and Engineering
Stanford University, Stanford, CA 94305

January 1991

Department of MATERIALS SCIENCE AND ENGINEERING
STANFORD UNIVERSITY

REPORT DOCUMENTATION PAGE

Form Approved
OMB No. 0704-0188

1. AGENCY USE ONLY (Leave blank)	2. REPORT DATE	3. REPORT TYPE AND DATES COVERED
	January 30, 1991	Annual Technical Report 11/89-11/90

4. TITLE AND SUBTITLE

High Temperature Deformation Processes and Strengthening Mechanisms in Intermetallic Particulate Composites

5. FUNDING NUMBERS

AFOSR No. 89-0201

6. AUTHOR(S)

William D. Nix

7. PERFORMING ORGANIZATION NAME(S) AND ADDRESS(ES)

Department of Materials Science & Engineering
Stanford University
Sanford, CA 94305

8. PERFORMING ORGANIZATION REPORT NUMBER

AFOSR - 91-2

9. SPONSORING / MONITORING AGENCY NAME(S) AND ADDRESS(ES)

Directorate of Electronic and Materials Sciences
AFOSR
Dept. of the Air Force
Bolling AFB D.C. 20332

10. SPONSORING / MONITORING AGENCY REPORT NUMBER

2306/A1

11. SUPPLEMENTARY NOTES

ATTN: Dr. Alan H. Rosenstein

12a. DISTRIBUTION / AVAILABILITY STATEMENT

unclassified/unlimited

12b. DISTRIBUTION CODE

13. ABSTRACT (Maximum 200 words)

Research on the high temperature deformation processes and strengthening mechanisms in Intermetallic Particulate Composites is described. Work during the second year of the grant includes high temperature compression tests of Ni_3Al - Al_2O_3 composites; mechanical alloying of Ni_3Al + Y_2O_3; transient deformation studies of the intermetallics Ni_3Al, NiAl, and NiBe; and development of a model of dislocation structure control of plastic deformation.

14. SUBJECT TERMS

15. NUMBER OF PAGES
38

16. PRICE CODE

17. SECURITY CLASSIFICATION OF REPORT	18. SECURITY CLASSIFICATION OF THIS PAGE	19. SECURITY CLASSIFICATION OF ABSTRACT	20. LIMITATION OF ABSTRACT
Unclassified	Unclassified	Unclassified	None

GENERAL INSTRUCTIONS FOR COMPLETING SF 298

The Report Documentation Page (RDP) is used in announcing and cataloging reports. It is important that this information be consistent with the rest of the report, particularly the cover and title page. Instructions for filling in each block of the form follow. It is important to ***stay within the lines*** to meet ***optical scanning requirements***.

Block 1. Agency Use Only *(Leave blank)*.

Block 2. Report Date. Full publication date including day, month, and year, if available (e.g. 1 Jan 88). Must cite at least the year.

Block 3. Type of Report and Dates Covered. State whether report is interim, final, etc. If applicable, enter inclusive report dates (e.g. 10 Jun 87 - 30 Jun 88).

Block 4. Title and Subtitle. A title is taken from the part of the report that provides the most meaningful and complete information. When a report is prepared in more than one volume, repeat the primary title, add volume number, and include subtitle for the specific volume. On classified documents enter the title classification in parentheses.

Block 5. Funding Numbers. To include contract and grant numbers; may include program element number(s), project number(s), task number(s), and work unit number(s). Use the following labels:

C	- Contract	PR	- Project
G	- Grant	TA	- Task
PE	- Program Element	WU	- Work Unit Accession No.

Block 6. Author(s). Name(s) of person(s) responsible for writing the report, performing the research, or credited with the content of the report. If editor or compiler, this should follow the name(s).

Block 7. Performing Organization Name(s) and Address(es). Self-explanatory.

Block 8. Performing Organization Report Number. Enter the unique alphanumeric report number(s) assigned by the organization performing the report.

Block 9. Sponsoring/Monitoring Agency Name(s) and Address(es). Self-explanatory.

Block 10. Sponsoring/Monitoring Agency Report Number. *(If known)*

Block 11. Supplementary Notes. Enter information not included elsewhere such as: Prepared in cooperation with...; Trans. of...; To be published in.... When a report is revised, include a statement whether the new report supersedes or supplements the older report.

Block 12a. Distribution/Availability Statement. Denotes public availability or limitations. Cite any availability to the public. Enter additional limitations or special markings in all capitals (e.g. NOFORN, REL, ITAR).

DOD	-	See DoDD 5230.24, "Distribution Statements on Technical Documents."
DOE	-	See authorities.
NASA	-	See Handbook NHB 2200.2.
NTIS	-	Leave blank.

Block 12b. Distribution Code.

DOD	-	Leave blank.
DOE	-	Enter DOE distribution categories from the Standard Distribution for Unclassified Scientific and Technical Reports.
NASA	-	Leave blank.
NTIS	-	Leave blank.

Block 13. Abstract. Include a brief *(Maximum 200 words)* factual summary of the most significant information contained in the report.

Block 14. Subject Terms. Keywords or phrases identifying major subjects in the report.

Block 15. Number of Pages. Enter the total number of pages.

Block 16. Price Code. Enter appropriate price code *(NTIS only)*.

Blocks 17. - 19. Security Classifications. Self-explanatory. Enter U.S. Security Classification in accordance with U.S. Security Regulations (i.e., UNCLASSIFIED). If form contains classified information, stamp classification on the top and bottom of the page.

Block 20. Limitation of Abstract. This block must be completed to assign a limitation to the abstract. Enter either UL (unlimited) or SAR (same as report). An entry in this block is necessary if the abstract is to be limited. If blank, the abstract is assumed to be unlimited.

Annual Technical Report
for
AFOSR Grant No. 89-0201

HIGH TEMPERATURE DEFORMATION PROCESSES AND STRENGTHENING MECHANISMS IN INTERMETALLIC PARTICULATE COMPOSITES

Submitted to :

Department of the Air Force
Directorate of Electronic and Materials Sciences
Air Force of Office of Scientific Research
Bolling Air Force Base, Building 410
Washington D.C. 20332

Attention: Dr. Alan Rosenstein

Submitted by:

Professor William D. Nix, Principal Investigator
Department of Materials Science and Engineering
Stanford University, Stanford, CA 94305

January 1991

This research was supported by the Air Force of Scientific Research (AFOSC) under Grant No. AFOSR-89-0201. Approved for public release; distribution unlimited.

Table of Contents

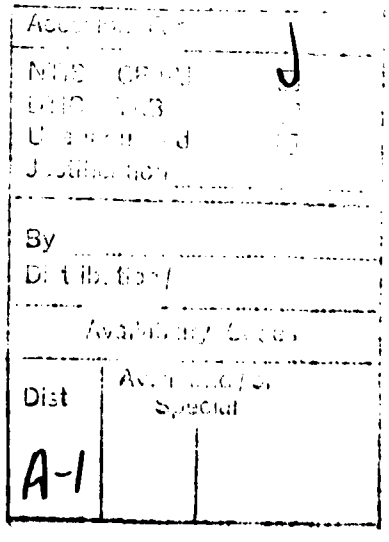

I. SUMMARY

A fundamental study of the high temperature deformation processes and strengthening mechanisms in intermetallic particulate composites is being conducted. The project is supported under AFOSR Grant No. 89-0201. In this report we describe some of the results of our research during the second year of this grant.

The aim of this research is to study and understand the deformation processes and strengthening mechanisms that operate in intermetallic particulate composites at high temperatures. As, indicated in our proposal, we will be studying both dispersion strengthened intermetallics and some single phase intermetallic alloys. Mechanical testing of these potentially brittle materials will be done in compression to avoid problems associated with premature failure. The development of an improved high temperature compression test apparatus was reported for the first year of this grant. During the past year, this apparatus was utilized in the testing of various single phase and particle strengthened intermetallic alloys.

Composites offer a simple approach to combing the beneficial properties of two materials. For example, the high temperature strength and integrity of a ceramic can be joined with the ductility of intermetallics at high temperatures. For our study, the high temperature mechanical properties of composites of the intermetallic Ni_3Al and the ceramic Al_2O_3 were evaluated in compression tests. The composites were found to have strength and ductility intermediate to those of the individual constituents. The strength the composite made from a 50 per cent mixture of Ni_3Al with Al_2O_3 was found to be superior to that of composites with less Ni_3Al. The mechanism of strengthening for this composite is not yet well understood though we suggest a possible interpretation.

Particle strengthening offers another process for improving the properties of intermetallic alloys. We have chosen to study a Ni_3Al matrix, for which dislocation mechanisms have already been characterized, strengthened with Y_2O_3 particles. We have produced these materials by mechanical alloying and characterized their structure as a function of processing parameters.

We have continued our study of the dislocation mechanisms in Ni_3Al by performing various transient tests. A large stress exponent is measured in stress relaxation tests suggesting that only a small number of mobile dislocations contribute to the deformation of Ni_3Al. A model to describe deformation of Ni_3Al should thus not be made in terms of dislocation mobility but should instead be related to the stochastic motion of a relatively small number of highly mobile dislocations. Temperature drop tests after a stress relaxation also suggests that dislocation motion in Ni_3Al is not

a thermally reversible process since dislocation motion does not recommence immediately upon a large temperature decrease. We conclude that the formation and dynamic recovery of Kear-Wilsdorf locks should play an important role in the description of dislocation glide in Ni_3Al. The "kink source" model incorporates these ideas and best explain our transient results.

The intermetallics, NiAl and NiBe, having high melting temperatures and low densities are promising as a basis for the next generation high temperature structural materials. Compression tests have been performed at high temperatures to confirm the superior strength of these alloys. Transient tests are also being accomplished to characterize the controlling dislocation mechanisms. Preliminary results are presented and discussed in this report.

A model of dislocation motion has been developed to explain some of the transient results of experiments. The principles of this model are described using the properties of copper which has been well characterized. Our model predicts that a small number of very mobile dislocations control deformation in copper and that transient stress relaxation tests can reveal this characteristic. Stress relaxation tests in Ni_3Al show a similar response as copper though an accurate modelling of dislocation motion would be more difficult for Ni_3Al. The relationship with results from the model, however, confirms our suggestion that deformation in Ni_3Al is dislocation structure controlled and not dislocation mobility controlled. We suggest ways that this model can be more directly applied to Ni_3Al and to other intermetallics in order to provide another approach to understanding the creep properties of these alloys.

II. RESEARCH REPORT

A. High Temperature Compression Tests of Ni3Al - Al2O3 Composites

K. R. Forbes (Graduate Research Assistant)

The technical demands of high temperature structural components has stimulated the development of intermetallic compounds which are able to maintain high strengths at elevated temperatures. Ni3Al has been successfully used in selected intermediate temperature applications but is still not appropriate for higher temperatures. The variation in strength of a Ni3Al (Hf, B) alloy with temperature is shown in Figure 1. The strength of the alloy is maximum at about 750 °C but falls rapidly above this temperature. It is this rapid decrease in strength that disqualifies Ni3Al for high temperature applications.

Ceramic materials, on the other hand, have very high melting temperatures and can maintain their strength to temperatures much above that of intermetallics. The strength of single crystal Al2O3 is compared with the strength of Ni3Al at various temperatures in Figure 1. Ceramics, however, are

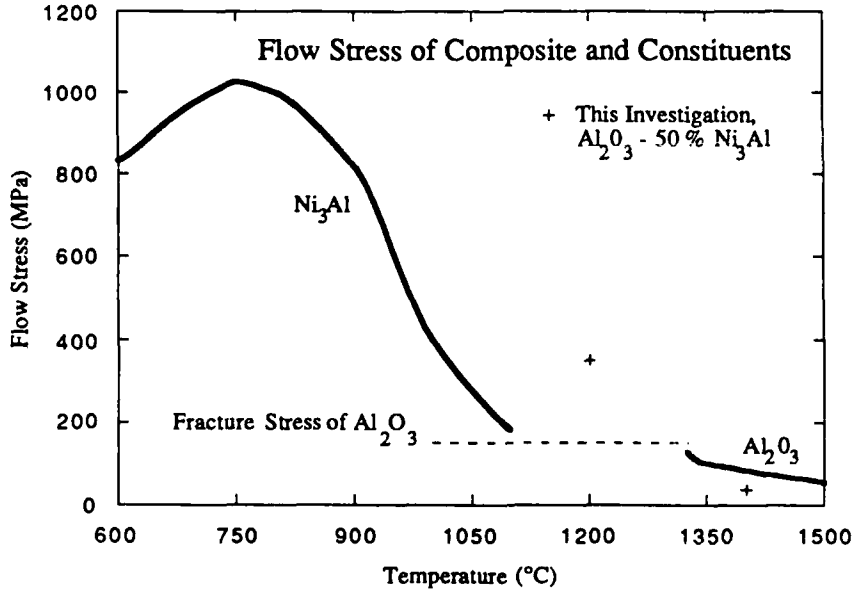

Figure 1. Comparison of the Flow Stress of Al2O3 - Ni3Al Composite and its Constituents. 0.2% Offset Yield Strength of Ni3Al from [1]. Yield Strength of Single Crystal Al2O3 from [2].

extremely brittle and thus inappropriate for many high temperature applications. A more ideal material would combine the ductility and strength of Ni_3Al with the high temperature integrity of a ceramic. A composite of Ni_3Al and a ceramic is the most direct approach to realizing the benefits of both in one material. The purpose of this investigation is to explore the enhancements offered by a Ni_3Al - Al_2O_3 composite over the properties of the individual constituents.

The composites for this study were provided by the Research and Development Division of the Lockheed Missiles and Space Company. The composites were made from mixtures of 75 μm particles of Ni_3Al (Hf, B) and 75 μm particles of Al_2O_3 at weight fractions of Ni_3Al equal to 0.17, 0.32 and 0.50. The mixtures were consolidated by hot pressing in a vacuum for 2 hours at 1200 °C under a 200 MPa load. Cylindrical samples, 4.5 mm diameter by 9 mm length, were cut from the pressed ingot.

The intermetallic composite samples were tested at room temperature and at 1200 and 1400 °C. A constant compressive strain rate of 10^{-4} s^{-1} was imposed while the load and displacement at the sample were measured. Elastic properties could not be measured during these compression tests; so, instead of more a typical representation of yield strength, the flow stress at 2% strain was used for comparison of the sample strengths. The stress-strain curves for these compression tests are show in Figure 2 and the value of the 2% offset yield strength are recorded in Table 1.

As expected, the composite has increased high temperature strength compared to Ni_3Al but lower strength than Al_2O_3. The strength of Al_2O_3 is significantly reduced with an addition of only 17 weight per cent Ni_3Al. Increasing the weight fraction of Ni_3Al to 32 per cent results decreases the strength of the composite insignificantly. The sample of 0.50 weight fraction Ni_3Al, however, has a greater strength then either of the samples with lower compositions. This is surprising since adding more of the lower strength Ni_3Al to the composition would suggest that the strength should decrease further. The 0.50 weight fraction composite also keeps much of its strength even to 1400°C which is slightly above the melting temperature of Ni_3Al (T_m = 1395°C).

Table 1. The 2% offset yield strength of Ni_3Al - Al_2O_3 composites at various test temperatures.

	Weight Fraction of Ni_3Al in composite		
Test temperature	0.17	0.32	0.50
27°C	fracture (300 MPa)	fracture (225 MPa)	fracture (300 MPa)
1200°C	120 MPa	110 MPa	250 MPa
1400°C	16 MPa	16 MPa	37 MPa

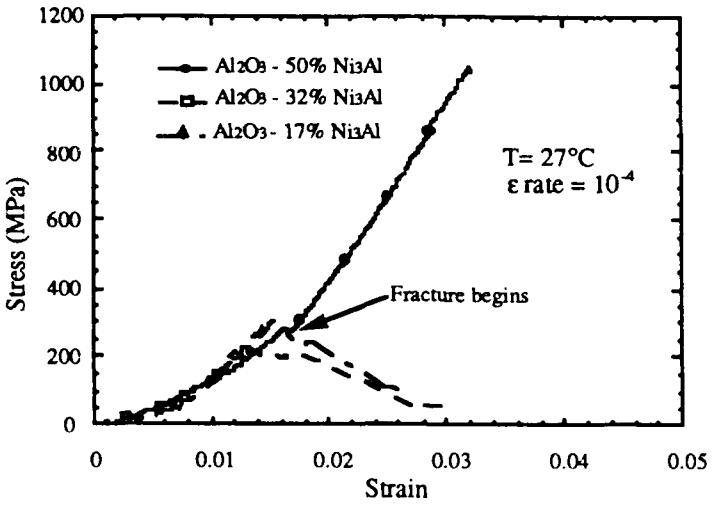

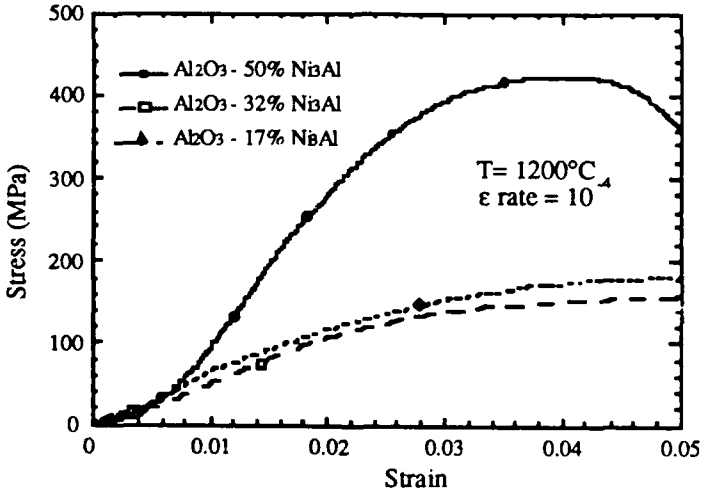

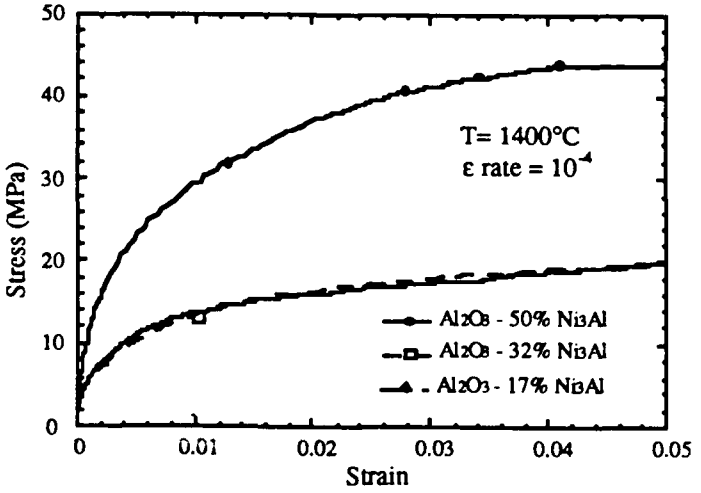

Figure 2. Stress-strain plots for Ni_3Al - Al_2O_3 composites at various temperatures.

The strength of the higher weight fraction samples suggests that larger fractions of Ni_3Al promote an additional phase between Al_2O_3 and Ni_3Al. Whereas small additions of Ni_3Al to Al_2O_3 results in a decrease in strength due to the weakening of the bonding between Al_2O_3 grains, an additional phase, if present, could somewhat strengthen the bonding between the ceramic grains. This postulation has yet to be tested by a more complete analysis of the composition of the matrix surrounding the ceramic grains.

The ductility of the composite, however, is much improved over that of the Al_2O_3. The ceramic fractures before yielding at temperatures below 1300 °C but the composites show no tendency to fracture except in the room temperature tests. Even the higher strength 0.50 weight fraction sample shows no loss of ductility.

In Figure 1, the yield strength of the strong 0.50 composite is plotted along with the strengths of Ni_3Al and single crystal Al_2O_3. The strength of the composite is greater than that of the intermetallic component though less than that of the ceramic component; and its ductility is much increased over the ceramic. Thus, Ni_3Al - Al_2O_3 composites show promise for high temperature applications although at present the strengthening mechanisms are not well understood.

References

1. R. S. Bellows and J. K. Tien, *Scripta Metall.* **21**, 1659 (1987).
2. M. L. Kronberg, *J. Am. Ceram. Soc.* **45**, 274 (1962).

B. Mechanical Alloying of Ni_3Al–Y_2O_3 Particulate Composites

D. D. Sternbergh (Graduate Research Assistant)

Introduction

Its increasing strength with temperature has made Ni_3Al an attractive material for structural applications at intermediate temperatures. However, the yield strength reaches a maximum around 750°C; above this point it drops sharply with temperature. Dispersion strengthening has been used successfully in a number of materials to help maintain mechanical strength at high temperatures. We are investigating the effects of oxide dispersoids on the strength of intermetallic Ni_3Al at intermediate and high temperatures.

Our model system is Ni_3Al containing a fine, uniform dispersion of yttrium oxide particles. A microstructure of this kind is difficult or impossible to achieve by conventional melting and solidification techniques. For this reason these materials are usually prepared using solid state and powder metallurgical processing techniques. We have prepared these materials by mechanical alloying, a solid state processing technique developed for producing composite metal powders with controlled, extremely fine microstructures.

Mechanical alloying is a high energy, dry ball milling process in which metal powder particles are repeatedly welded, fractured and rewelded.[1] The initial powder size is relatively coarse on the scale of the desired microstructure, but as powder particles are flattened in ball-particle-ball collisions the distance between surfaces is greatly reduced. Although the size of the average powder particle remains relatively coarse throughout the process, the characteristic dimension of heterogeneity within each metal powder particle is reduced from the initial particle size to sub-micron dimensions. In some systems chemical homogeneity on the atomic scale may be achieved.

Successful mechanical alloying depends both on the ability of the powder particles to cold-weld to each other and to fracture. The concurrent processes of welding and fracture must be balanced in order to achieve the desired microstructure. If fracture were dominant, the powders would be reduced in size to the limit of comminution, on the order of microns, but none of the necessary mixture on the nanometer or atomic scale would occur. If, on the other hand, welding were to dominate, the powders would quickly agglomerate or weld to the sides of the container and processing would halt. One of the physical characteristics of the starting powders which is important in establishing the critical welding-fracture balance is their brittleness or ductility. This consideration led us to choose two different systems to process: pure elemental nickel and

aluminum powders for a relatively ductile system, and pre-alloyed ordered Ni_3Al powders for a relatively brittle system.

To follow the relative rate of welding versus fracture, and to establish when the processing had reached a steady state, we determined the size distribution of the particles as a function of processing for each system.

Because the introduction of oxide particles, even at small volume percentages, can slow the processing rate by as much as a factor of four in some systems [2] we conducted a comparison of each system both with and without the addition of 3.2 vol.% Y_2O_3 particles.

Although the material will have an ordered superlattice structure after consolidation and annealing, the effects of earlier processing may well affect the microstructure and hence the mechanical properties of the final material. Mechanical alloying can produce thermodynamically stable ordered structures in β-brass [2] and some nickel aluminides; [3] in other systems it will produce highly supersaturated solid solutions. It has even been used to form amorphous structures in a number of systems such as Nb_3Sn and Ni–Zr alloys. We have used X-ray diffraction to monitor for the presence, appearance, or disappearance of order in both the intermetallic powder and the elemental powder series. In addition we have tried to measure the incorporation of aluminum in supersaturated solid solution in a nickel matrix.

Experimental Procedure

The nickel powder used in this study was obtained from Aesar, 99.9% pure, 3–7 μm particle size. The aluminum powder was from Fisher Scientific, 99%, 15–25 μm. The yttrium oxide was from Alfa Inorganics, 99.99%. The intermetallic powder was the alloy IC-50, kindly provided by Dr. C. T. Liu. It's composition was Ni–11.70Al–0.89Zr–0.02B (wt.%), screened to –100+200 (74–149 μm).

Mechanical alloying was performed with a SPEX 8000 Mixer/Mill using hardened steel cans and balls for milling media at a ball to powder weight ratio of 6.6:1. The temperature was not controlled during the milling process.

Metallographic specimens were mounted in Bakelite, polished to 0.5 μm diamond grit on polyester film, and etched with Keller's reagent for 5–10 sec. We used a set of Bel-Art microsieves to determine the distribution of particle sizes.

X-ray diffraction was performed on powder samples using Cu K_α radiation.

Experimental Results

Optical Microscopy

Ni, Al Elemental Powders: Optical micrographs of the elemental starting materials are shown in Figure 1. Figures 2 and 3 show processed materials without and with oxide particles respectively. Even from the micrographs the evolution of powder particle size is evident: rapid growth in size as welding predominates followed by refinement as particles are comminuted.

Figure 1: Optical micrograph of starting powders. The large aluminum particles have been mottled by a Keller's reagent etch; the smaller nickel particles are relatively featureless.

The structural development in the elemental powders can be seen clearly in the micrographs. At 30 min. (Fig. 2a and 3a) the particles have a laminated structure. In these initial stages of processing, the ductile particles are flattened during collisions and cold-welded to other flattened particles. They tend to be much larger in size than the initial starting powders, and the layers are roughly parallel. At 90 min. (Fig. 2b and 3b) the lamellar features are still visible, although the inter-layer spacing has decreased. After 270 min. the powders without oxide (Fig. 2c) are optically homogeneous and featureless. At 300 min. (Fig. 3c) the powders with oxide are almost completely lacking visible features. A small percentage have features which are barely discernible. At this point it is usually assumed that the spacing between oxide particles on adjacent prior surfaces is approximately the same as the spacing between adjacent particles on the same prior surface, i.e. the oxide particles are uniformly distributed throughout each metal powder particle

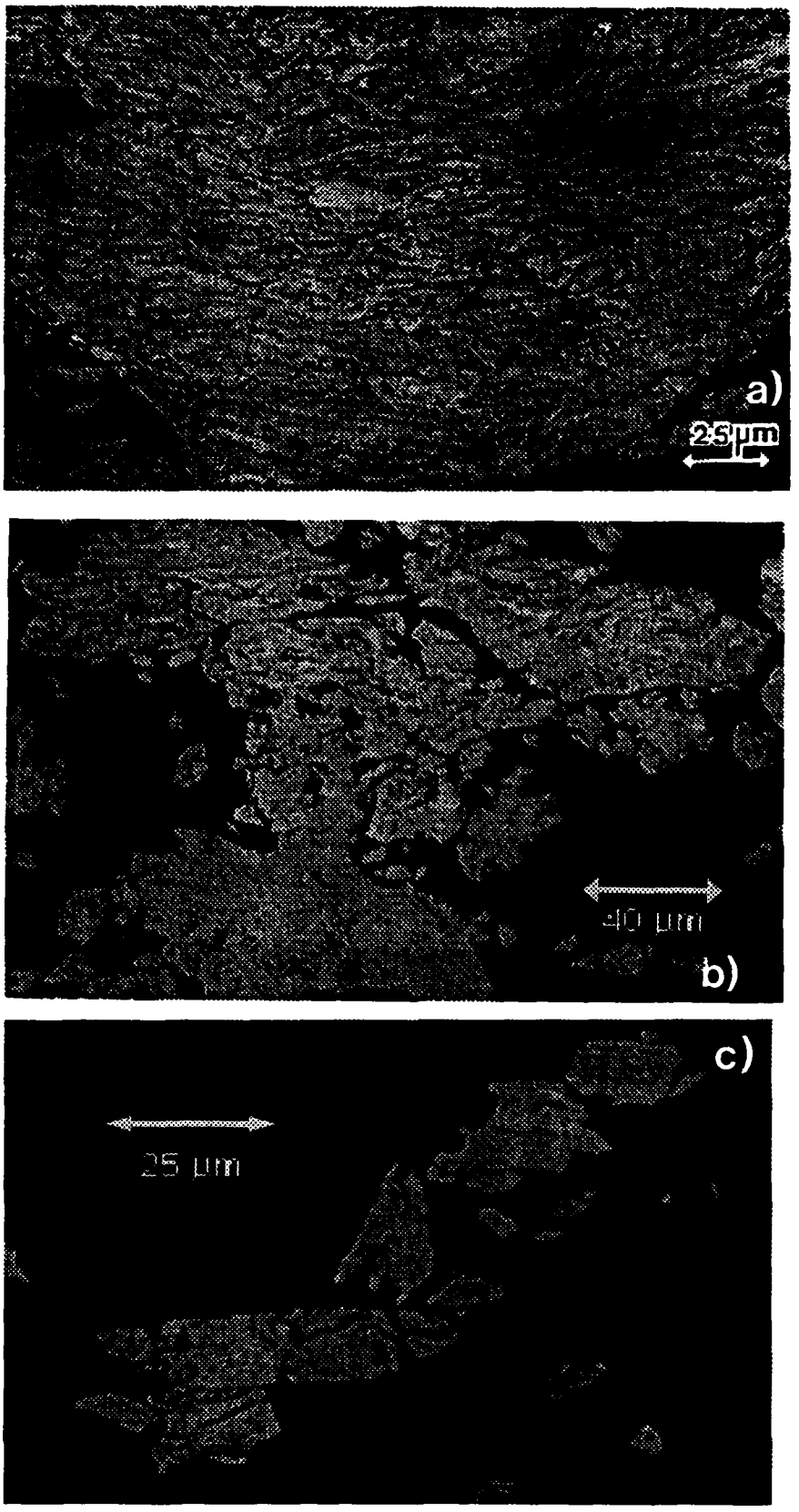

Figure 2: Micrographs of Ni–25at.% Al mechanically alloyed for (a) 30 minutes, (b) 90 minutes, and (c) 270 minutes.

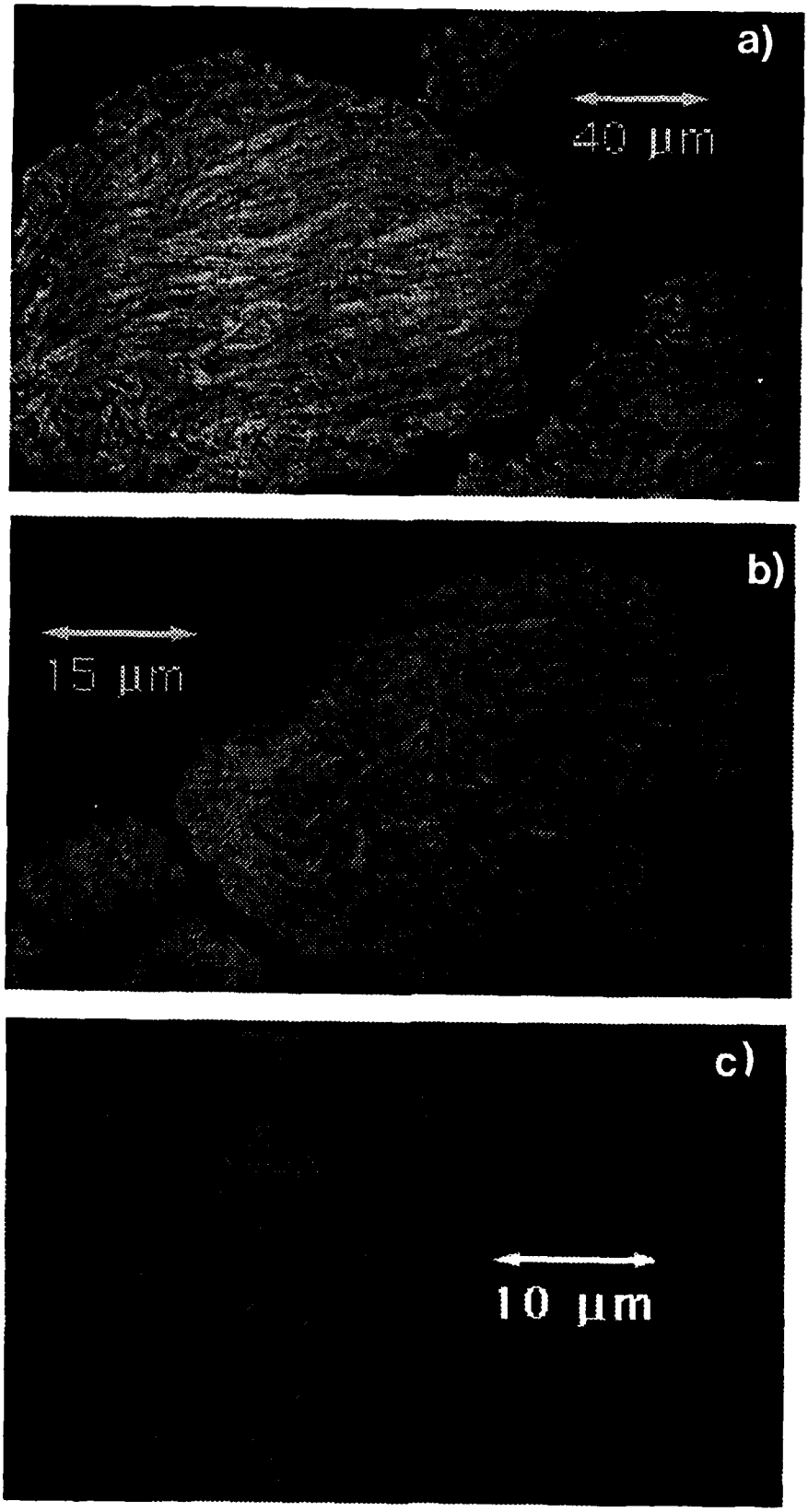

Figure 3: Micrographs of Ni–25at.% Al mechanically alloyed for (a) 30 minutes, (b) 90 minutes, and (c) 270 minutes.

(cf. Fig. 4). This stage of processing is referred to as "steady state," since no further developments in the microstructure are expected or observed. We note that the presence of oxide particles has no significant effect on the time required to reach this state.

Particle Size Distribution

Elemental Powders: The distribution of particle sizes are compared in Fig. 5 and Fig. 6. In Fig. 5 we show the initial size distribution of the elemental powders. After 30 minutes of processing, a very large fraction of the powder is retained on the coarser screens. Some portion of these particles have the same volume as the initial particles and have simply been flattened into flakes. However, the majority of these particles consist of several original particles flattened and subsequently cold-welded to form equiaxed particles much larger than any of the starting constituents. This effect is seen in both the powder charges with oxide and without oxide, although the oxide-containing powders are shifted to smaller particle sizes. At longer processing times (300 min. and 810 min.) the fracture process has reduced the size of the particles greatly to a roughly steady state distribution.

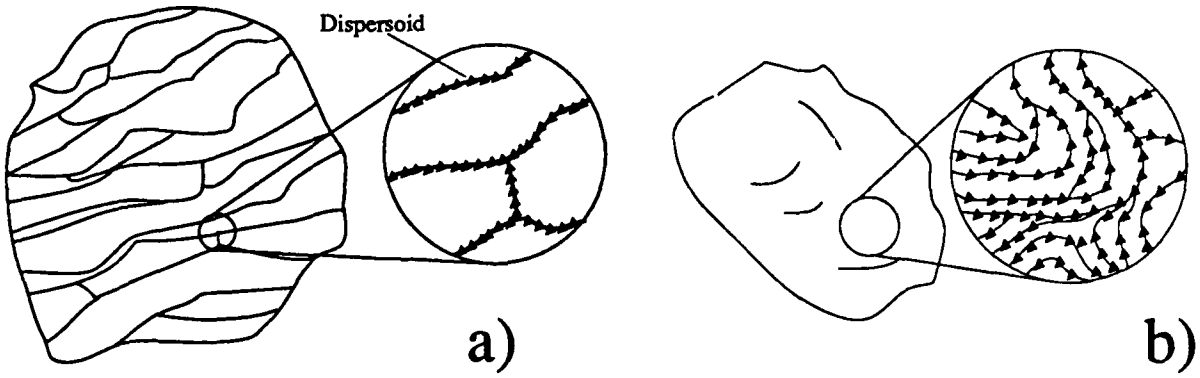

Figure 4: Schematic illustration of mechanical alloying during (a) initial stages, and (b) advanced stages. In the early stages, (a), the structure is arranged in parallel layers. Dispersoids are located along prior-surface boundaries. Later in processing, (b), the layers are very convoluted and cannot be resolved optically. The distance between the boundaries is comparable to the distance between adjacent oxide particles.

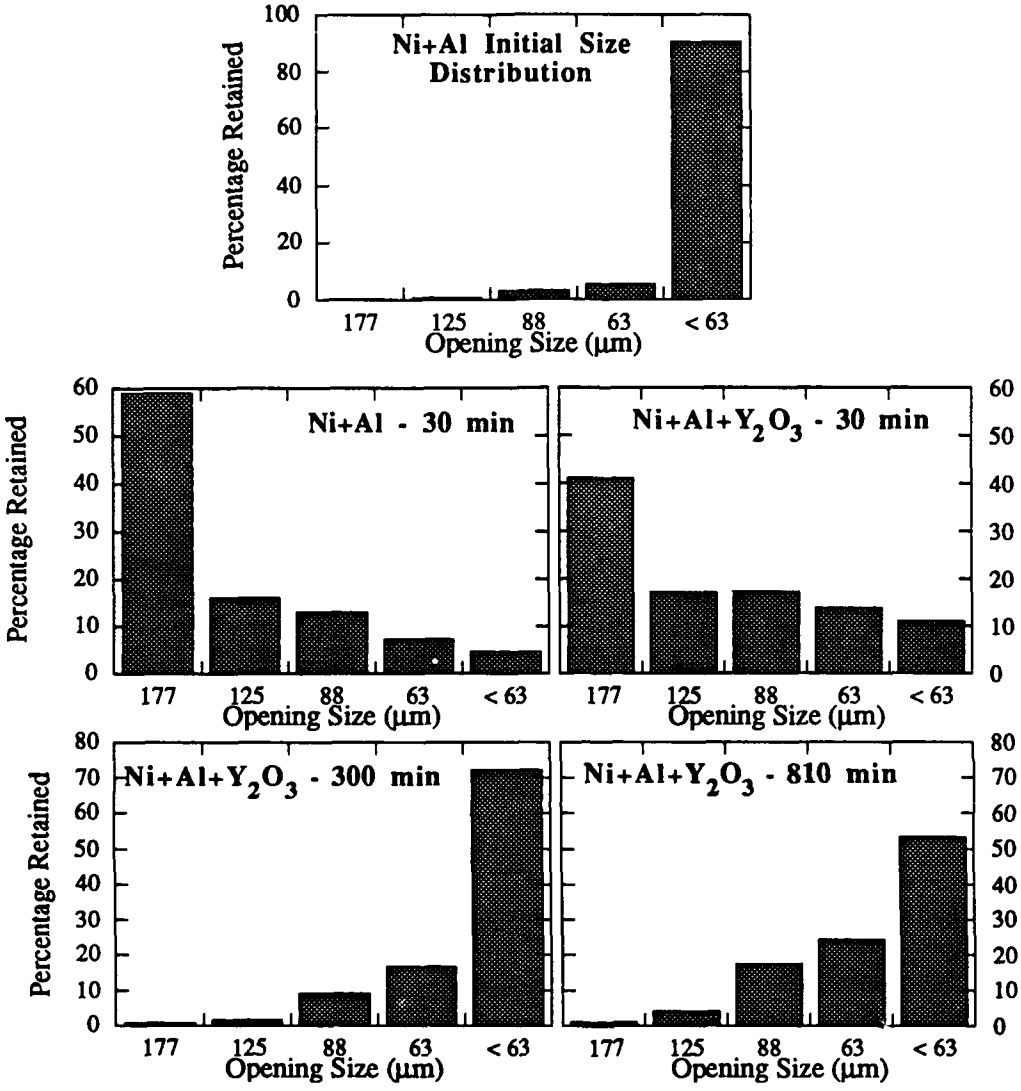

Figure 5: The distribution of particle sizes for elemental starting materials and processed powders at various processing times.

Pre-Alloyed Intermetallic Powders: In Fig. 6 we present the initial size distribution of the intermetallic powder particles, screened to –100+200. Again after 30 minutes of processing, a significant fraction of larger, welded particles have been produced in both the system without oxide and that with oxide added. In addition, a substantial quantity of particles smaller than the powders in the initial charge are found. Fracture is occurring at an appreciable rate in these more brittle powders, even in these early stages of processing. At longer times, the size distribution is considerably refined, especially for the powders with oxide particles. Although in all cases powders processed with oxide particles had smaller powder particle sizes, the development trends

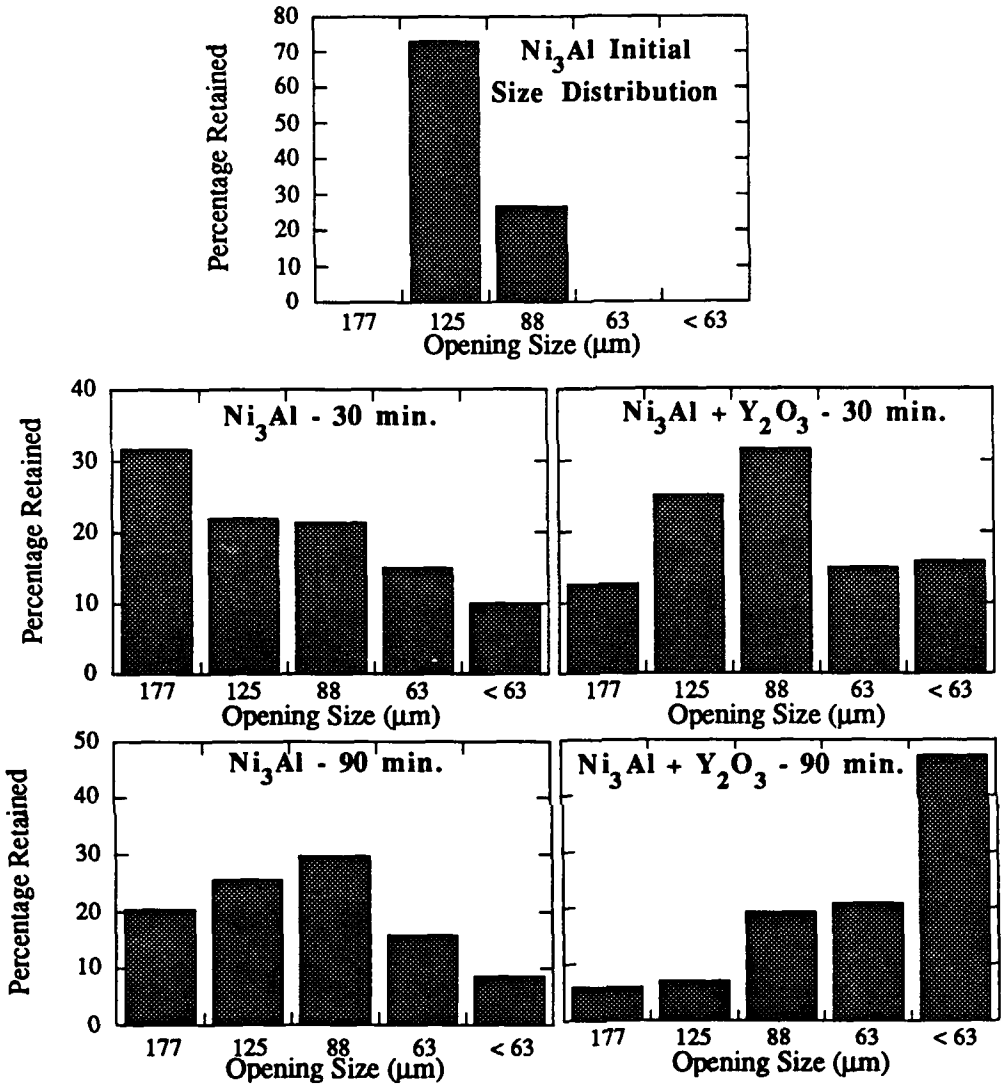

Figure 6: The distribution of particle sizes for pre-alloyed intermetallic starting materials and processed powders at various processing times.

were identical and, consistent with the observations of optical metallography, there was no significant difference in time required to reach a "steady state" distribution.

We do note that one important piece of information is not conveyed by the size distribution: the relative sizes are reported, but the absolute yield cannot be. This is only important in the case of the intermetallic powder processed without oxide for 810 min. Yield under these conditions was exceedingly small, too small to provide a distribution. Most of the powder had welded to the milling media, behavior more characteristic of ductile elements milled for short times. This behavior was reproducible and markedly different from the same material processed with oxides.

This is an indication that the "steady state" thought to be achieved with sufficient processing is, in fact, not a true steady state, although parameters of interest such as oxide particle spacing or spatial distribution of chemical constituents may not be changing. To our knowledge this observation has not previously been reported.

X-ray Diffraction

X-ray diffraction scans of the intermetallic powder (without oxide) are shown in Fig. 7. Superlattice peaks indicative of the long range order of the alloy are seen from the powders as received. We are not able to see evidence of long-range order after even short processing times.

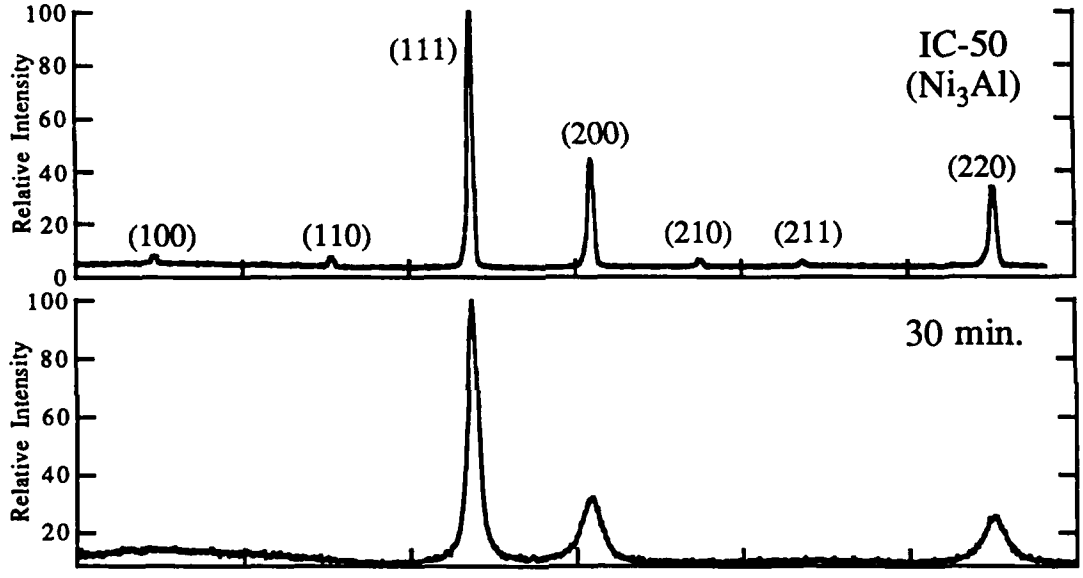

Figure 7: X-ray diffraction scan of IC-50 powder as received and after 30 minutes of processing. The peaks of mixed indices (e.g. 100), normally absent in FCC materials, are evidence of the long range order. After 30 minutes of processing, these peaks are not evident, indicating that the long range order has been significantly reduced.

X-ray diffraction was also used to measure the lattice parameter of the nickel phase. As larger aluminum atoms are incorporated into the nickel in substitutional solid solution, the lattice parameter of the nickel phase should increase. Extrapolating linearly beyond the limits of solid solubility, we should be able to measure the amount of aluminum dissolved in the nickel. Although systematic errors have made our results inconclusive at this time, early results have shown the promise of this technique for measuring the formation of a supersaturated solution of aluminum in nickel by mechanical alloying

Continuing Work

We are currently consolidating the powders to form samples for compressive mechanical testing. We will test these samples to determine not only their basic creep properties at intermediate and high temperatures, which will be of significant interest, but more importantly to determine the strengthening mechanisms at work. Transient tests, current work in which is described below, will tell us about the dislocation mechanisms which are active. By combining transient tests in imaginative ways, as we have done with single crystal Ni_3Al below, we will extend our understanding of the interactions of these dislocation mechanisms with the strengthening dispersoids. We expect the presence of oxide particles to have a profound effect on the dislocation structure factor, the key to the anomalous yield strength in Ni_3Al. One objective will be to determine whether departure-side pinning is an important factor in strengthening these extended-dislocation-core materials.

Conclusions

1. Mechanical Alloying reaches optical homogeneity in ~4 ½ hours for elemental nickel and aluminum powders.

2. The presence of Y_2O_3 promotes fracture and inhibits welding, but does not significantly affect the processing rate.

3. Although the parameters of interest may not be changing, the state achieved at longer processing times is not a true steady state.

4. No evidence of ordering was observed in Ni_3Al powders even at short (30 min.) processing times.

5. X-ray measurements of Ni(Al) solid solution are inconclusive, but the technique is promising.

References

1. J. S. Benjamin and T. E. Volin, *Met. Trans.* **5**, 1929 (1973).
2. T. K. Wassel and L. Himmel, US Army Tank-Automotive Command Report No. 12571 (1981).
3. E. Ivanov, T. Grigorieva, G. Golubkova, V. Boldyrev, A. B. Fasman, S. D. Mikhailenko and O. T. Kalinina, *Materials Letters* **7**, 51 (1988).

C. Transient Deformation in the Intermetallic Alloy, Ni_3Al

K.J. Hemker, K.R. Forbes, D.D. Sternbergh (Graduate Research Assistants)

Introduction

The yield strength anomaly of Ni_3Al has been studied extensively and it is generally accepted that the increase in the critical resolved shear stress (CRSS) with temperature involves primary octahedral glide which is retarded by "cross-slip" onto the (010) plane. By comparison, very little attention has been paid to the creep properties of Ni_3Al. It has been observed [1,2] that the creep strength of Ni_3Al decreases with increasing temperature in the region where the CRSS increases with temperature, but the dislocation mechanisms that control the creep behavior have only recently been identified [2]. It has been shown that octahedral glide is exhausted during primary creep and that most of the creep deformation following this exhaustion process is caused by the bowing out and gliding of dislocations on the (010) cube cross-slip plane. The observation of octahedral glide during primary creep suggests that yielding and primary creep are related processes.

While it is widely believed that anomalous yielding is associated with the inhibition of octahedral glide by cross-slip onto the (010) plane. Several dislocation models have been proposed [3-8], but the exact mechanism by which the formation of cross-slipped segments leads to the observed increase in CRSS has not been conclusively identified. Most of the experiments that have been conducted to identify the controlling mechanisms for octahedral glide in Ni_3Al have been constant strain-rate experiments. By contrast, very few creep experiments and even fewer transient deformation experiments have been conducted. A viewpoint of the present investigation is that the information derived from constant strain rate deformation experiments is incomplete and that other kinds of deformation experiments are needed to provide a more complete picture of the controlling mechanism.

Deformation transients associated with changes in stress and strain-rate have proven to be useful in the determination of the controlling deformation mechanisms in various metals and alloys [9-11]. In like manner, the transient experiments which are described in this work have been designed to provide a more complete description of the deformation of Ni_3Al. These transient experiments include stress relaxation experiments and deformation exhaustion / temperature reduction tests. A picture of octahedral glide which is consistent with the results of these transient experiments has been developed and will also be presented.

Experimental Procedures

A detailed description of the experimental procedures for the creep experiments is given elsewhere [2]. Single crystals of single phase Ni_3Al (Ta) with a composition of Ni - 24.0 Al, 1.0 Ta (atomic %) were grown for the transient experiments by J.R. Whetstone and D. Frasier of the Allison Gas Turbine Division of General Motors. Parallelepiped compression specimens with a specimen orientation of [-0.95, 2.15, 3] were electrode discharge machined from the crystals. The transient experiments were all conducted in the temperature range (25-500° C) where the CRSS is known to increase with increasing temperature. Temperature change experiments were conducted between 500 and 100° C, and the stress relaxation and exhaustion / temperature reduction experiments were conducted at 300° C. All strain-rate controlled experiments were conducted at a true strain rate of 4×10^{-4} (1/sec). The stress relaxation experiments were conducted by fixing the displacement of the cross head after 3 % plastic strain, and the stress relaxation / temperature drop experiments were performed while the stress was held constant by computer control. All displacements were measured by a symmetrical LVDT system which was attached to the ceramic platens that apply load to the specimen.

Deformation Transient Experiments

Stress Relaxation Experiments. Materials in which flow is controlled by dislocation mobility are generally acknowledge to be very strain rate sensitive and are usually characterized by a large strain rate exponent (m) and a low stress exponent (n). However, the effect of strain rate on the flow stress of Ni_3Al as measured in constant strain rate experiments has been shown to be negligible [12]. In order to determine if dislocation mobility plays an important role in determining the flow stress, stress relaxation experiments have been conducted to measure the effects of stress and strain rate on the flow properties of Ni_3Al.

The stress exponent (n) and the activation volume (V_{act}) are deformation parameters that can be used to identify the microstructural mechanisms that control deformation. Stress exponents (n) and activation volumes (V_{act}) for various materials at low temperatures are given in Table II. From this table, it can be seen that for materials in which dislocation mobility controls deformation (i.e. solid solution alloys and bcc metals) typical values of n and V_{act} are 5 and 100 b^3 respectively. By comparison, materials in which deformation is controlled by the dislocation substructure, (i.e. pure fcc metals and Class II solid solution alloys) have values for n and V_{act} that are closer to 100 and 2000 b^3.

Table 2: Typical Values of Stress Exponents (n) and Activation Volumes (V_{act})

	Materials	Ref.	n	V_{act} (b^3)
Dislocation Mobility Controlled	Nb	(i)	5–7	50
	LiF	(i)	5–7	140
	W	(i)	5–9	5
Dislocation Obstacle Controlled	Zn	(ii)	50–100	—
	Cu	(iii)	100	2000
	Ag	(iv)	300	1770

(i) J.C.M. Li, "Kinetics and Dynamics in Dislocation Plasticity", in Dislocation Dynamics, Eds: A.R. Rosenfield, G.T. Hahn, A.L. Bement, Jr. and R.I. Jaffee, McGraw-Hill, New York (1968). p.87.
(ii) K.H. Adams, T. Vreeland, Jr. and D.S. Wood, Mater. Sci. and Engr., **2**, 37 (1967).
(iii) J. Bonneville, B.Escaig and J.L. Martin, Acta Metall., **36**, 1989 (1988).
(iv) H. Mecking and U.F. Kocks, Acta Metall., **29**, 1865 (1981).

The curve given in Fig. 1 (a) is representative of the stress relaxation curves that were obtained in this study. The observation that the strain rate drops to a very low value with very little change in stress suggests that dislocations are immobilized very quickly. We believe this occurs by the formation of KW locks. As is shown in Fig. 1 (b), the stress exponent (n) for Ni_3Al was determined to be 200. Comparing this value with the materials listed in Table II suggests that deformation of Ni_3Al should not be considered as dislocation mobility controlled but rather should be considered dislocation obstacle controlled. This "pure metal like" behavior suggests that a small number of highly mobile dislocations carry the deformation and that most of the dislocations are sessile and are a part of the dislocation substructure, *i.e.* in the form of KW locks.

Stoiber *et al.* [13] have conducted similar stress drop experiments in order to determine the activation volume of Ni_3Al. Results from their work indicate that the activation volume for Ni_3Al (1% Ta) is about 2000 b^3. This value is in good agreement with the experiments that were conducted in the present work, and the results of both stress relaxation experiments suggest that the reversible part ot the flow stress is not caused by a reduction of the dislocation mobility, but is instead related to the strain that a dislocation can produce before it cross-slips and forms a KW lock.

Relaxation / Temperature Drop Experiments. If dislocation motion in Ni_3Al is a thermally reversible process then the exhaustion observed in the stress relaxation experiments and during primary creep should be reversible. Specifically, a decrease in temperature should bring about an immediate increase in dislocation motion and the observation of additional plastic strain. However, if the dislocation motion in Ni_3Al is at least partially inhibited by the formation of KW locks, a decrease in temperature will not lead to an increase in dislocation motion because the formation of

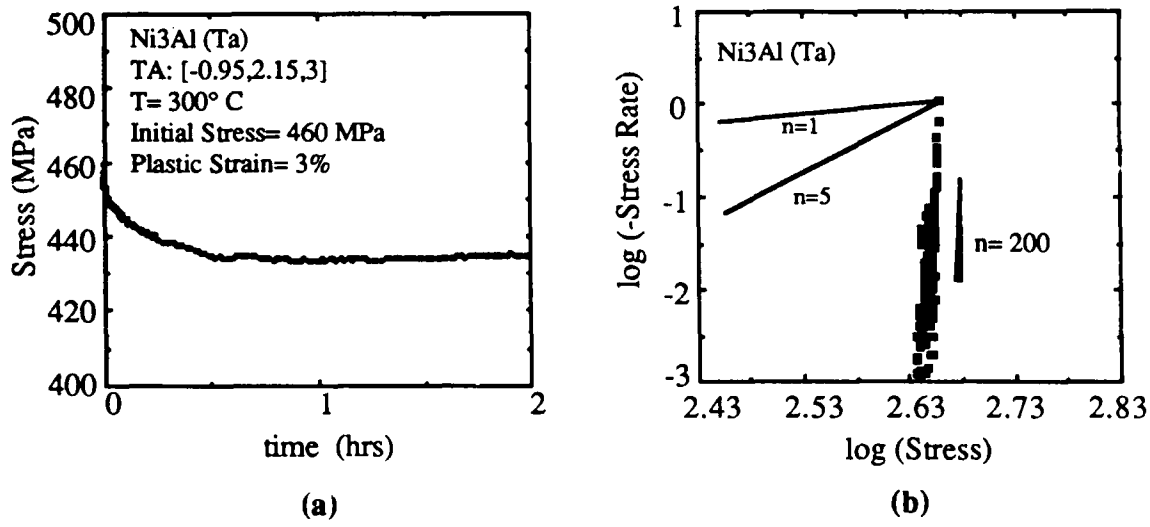

Fig. 1: (a) A stress relaxation experiment for Ni_3Al (Ta). The relaxation exhausts after a 6% decrease in stress, and (b) the low temperature stress exponent was determined to be 200. Comparing this value with the data in Table II suggest that flow in Ni_3Al is not dislocation mobility controlled but is instead dislocation obstacle controlled.

KW locks is not a reversible process. Reducing the temperature after a stress relaxation experiment, or after the exhaustion of primary creep, without accumulating additional plastic strain could be taken as a strong indication that dislocation motion in Ni_3Al is only a partially recoverable process and that the formation of KW locks play an important role in determining the flow stress.

A constant strain rate experiment was conducted at 300° C with the specimen being deformed to 2.0 % plastic strain. The cross head was then stopped and the specimen was allowed to relax for 2 hours while the drop in stress was monitored. At this point, the test was switched to constant stress control and the temperature was decreased while the strain was monitored. In a similar experiment, a constant stress of 330 MPa was applied to a creep specimen and the specimen was allowed to deform at 300° C until octahedral glide was exhausted. After this time (24 hours), the furnace was turned off and the strain was monitored as the temperature was allowed to drop. As is shown in Fig. 2 the temperature was reduced by approximately 40° C in the yielding experiment and 30° C in the creep experiment before any change in strain was observed. This drop in temperature without a corresponding increase in strain is taken as an indication that octahedral glide is not a completely recoverable process and that the formation of KW locks during primary creep has an important effect on the flow properties of Ni_3Al.

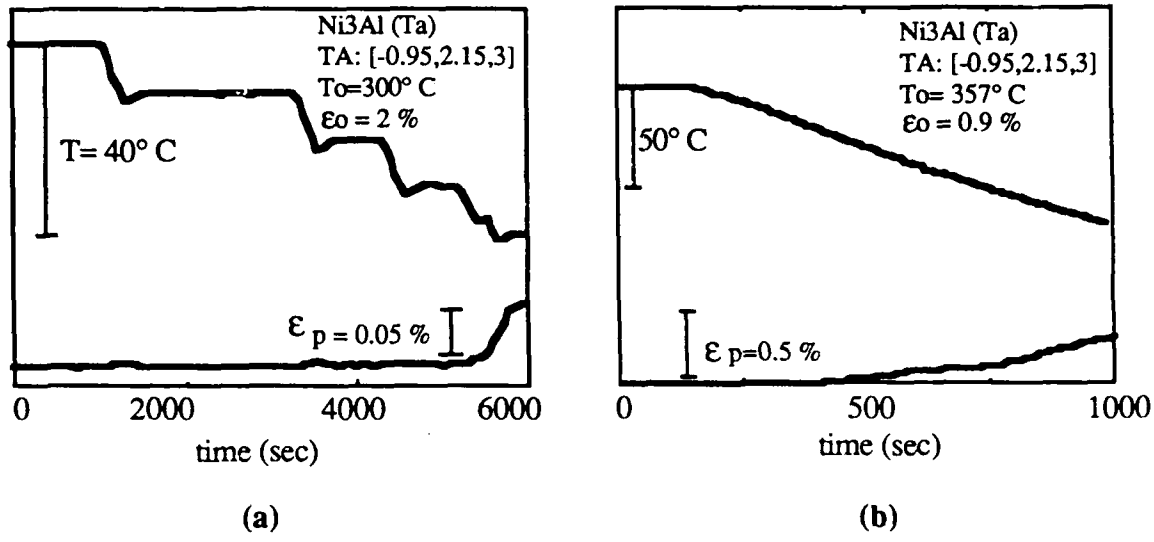

Fig 2: Deformation exhaustion / temperature drop experiments associated with **(a)** stress relaxations, and **(b)** primary creep. The observed decreases in temperature without a corresponding increase in plastic strain indicates that flow is only a partially reversible process.

A Description of Octahedral Glide Based on Transient Observations

The nature of dislocation motion can be characterized by the results of the stress relaxation experiments. The stress exponent (n=200) that was measured in this study and the activation volume (V_{act}=2000 b^3) that was reported by Stoiber, *et al.* [13] both indicate that octahedral glide in Ni_3Al is not dislocation mobility controlled but is instead dislocation obstacle controlled. In metals and alloys where dislocation motion is obstacle controlled (fcc metals and class II solid solution alloys) deformation is thought to be achieved by the rapid motion of a relatively small number of highly mobile dislocations. In this situation, dislocations are thought to be free to glide some free flight distance until they become tangled in the dislocation substructure, at which point the generation of new dislocations is required to continue deformation. It can be assumed that for Ni_3Al this free flight distance is determined by the frequency of cross-slip. If the frequency of cross-slip is taken to be dependent on temperature and specimen orientation in the manner that was described by Paidar *et al.* [4], the effects of temperature and orientation on the flow stress could be accounted for. In this way, octahedral glide can be viewed as a stochastic process that is not only consistent with the results of the stress relaxations experiments but also able to explain the temperature and orientation dependences that have been measured.

Some models that have been proposed to explain the anomalous yield strength have concentrated on the effects of cross-slip on the mobility of screw dislocations and neglected the effects of work

hardening and substructure formation. While it is clear that the cross-slip process is integral to the flow behavior, the results of the transient experiments suggest that this lack of provision for work hardening is a major deficiency in these models. The observation of a normal primary creep transient and the drop in temperature without a corresponding increase in plastic strain in the exhaustion / temperature drop experiments indicate that permanent obstacles are formed during deformation and that these obstacles play an important role in determining the flow strength of Ni_3Al.

In this work, strain hardening has been associated with the formation of KW locks. One of the major objections to the use of KW locks in a description of the flow strength anomaly lies in the fact that the continuous formation of KW locks would lead to the obstruction of octahedral glide. Without a sufficient recovery process the formation of KW locks would result in an extremely high strain hardening rate and the observation of correspondingly high flow stresses. In fact, the shape of the stress strain curve indicates that recovery occurs at relatively low temperatures, suggesting that it is dynamic recovery, not diffusive recovery, which must be operative. Dynamic recovery is usually associated with the cross-slip and subsequent annihilation of oppositely signed dislocations, but for Ni_3Al cross-slipped dislocations are sessile and unable to glide together and annihilate. An alternative description of dynamic recovery is needed for Ni_3Al.

The kink source process that was originally described by Mills *et al.* [7], and later included in the work of Sun [14], can account for the recovery of KW locks. Mills *et al.* suggested that the kink segments that lie on the (111) plane between the KW locks can bow out and glide on the (111) plane, and that in doing so these segments could annihilate a number of KW locks and allow the entire dislocation to glide forward until it cross-slips and becomes locked again. This kink expansion concept is attractive because it allows for the formation and recovery of KW locks that is needed to explain the work hardening observations and it is also consistent with both the stochastic nature of octahedral glide that is suggested from this study as well as the TEM observations that have been reported.

Conclusions:

1. The description of a critical stress for dislocation motion is not consistent with the observation of either primary creep or micro yielding.

2. The results of stress relaxation experiments suggest that the reversible part of the flow stress cannot be described in terms of dislocation mobility but should instead be related to the stochastic motion of a relatively small number of highly mobile dislocations.

3. Primary creep and the shape of the stress strain curve suggest that strain hardening, the formation of KW locks, plays an important role in determining the flow stress.

4. A complete description of octahedral glide that is based on the formation of KW locks must include a provision for the dynamic recovery of these locks.

5. In their present form, the yielding models that have been proposed to explain the yielding behavior of Ni_3Al are unable to explain all of the transient observations. The "kink source" model is able to explain a number of the transient observations and appears to be the best candidate for further development.

References

1. J.R. Nicholls, and R. D. Rawlings, *J. Mater. Sci.*,12, 2456, (1977).
2. K.J. Hemker, M.J. Mills, and W.D. Nix, submitted to *Acta Metall.*, (1990).
3. S. Takeuchi and E. Kuramoto, *Acta Metall.*, **26**, 207, (1978).
4. V. Paidar, D.P. Pope, and V. Vitek, *Acta Metall.*, **32**, 435, (1984).
5. Y.Q. Sun and P.M. Hazzledine, *Phil. Mag. A*, **58** (4), 603, (1988).
6. P. Veyssière, *Mat. Res. Soc. Symp. Proc.*, **133**, 175, (1989).
7. M.J. Mills, N. Baluc, and H.P. Karnthaler, *Mat. Res. Soc. Symp. Proc.*, **133**, 203, (1989).
8. D. Caillard, N. Clement, A. Couret, P. Lours, and A. Coujou, *Phil. Mag. Letters*, **58**, 263, (1988).
9. O.D. Sherby, R.H. Klundt and A.K. Miller, *Metall. Trans.* A, **8A**, 843 (1977).
10. D.L. Yaney, J.C. Gibeling and W.D. Nix, *Acta Metall.*, **35**, 1391 (1987).
11. A.H. Cottrell and R.J. Stokes, *Proc. Roy. Soc.*, **A233**, 17, (1955).
12. G.R. Leverant, W. Gell, and S.W. Hopkins, *Mater Sci. Eng.*, **8**, 125, (1971).
13. J. Stoiber, J. Bonneville and J.L. Martin, *Proc. 8th ICSMA* Ed: P.O. Kettunen, T.K. Lepistö and M.E. Lehtonen, Pergamon Press, Oxford, (1988).
14. Y.Q. Sun, PhD. Thesis, Oxford University, (1990).

D. Transient Experiments on NiAl, NiBe Intermetallic alloys

K. R. Forbes (Graduate Research Assistant)

Background

Although alloys of Ni_3Al have been more extensively developed, this is not the most promising of ordered intermetallics for use in high temperature applications. With a relatively low melting point (1390 °C) and high density (7.50 g/cm^3), Ni_3Al offers only a marginal improvement over current superalloy compositions. The intermetallic NiAl has a much lower density (5.86 g/cm^3) and a higher melting temperature (1640 °C) which could result in significant improvements over current alloys. However, polycrystalline NiAl is extremely brittle at room temperature and will require additional processing and alloying to produce a suitable structural material. NiAl exists over a large range of stoichiometry with a relatively constant creep strength which suggests that alloying is feasible to improve its mechanical properties. Whittenberger [1] has found that the flow stress of NiAl does not vary far from 30 MPa at 1300 K for a range of compositions between 43.9 and 52.7 atomic per cent Al.

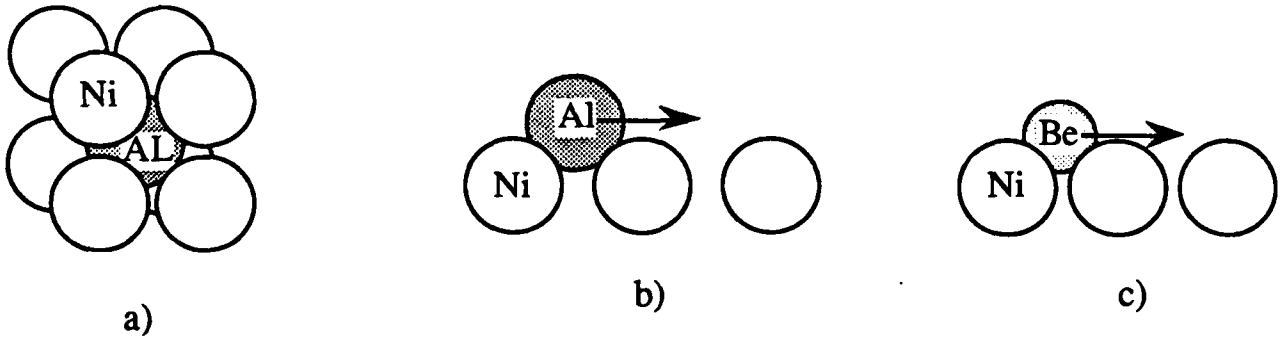

Figure 1. **a)** A unit cell of ordered NiAl with the B2 crystal structure. **b)** An approximation of the relative position of an Al atom in NiAl compared with **c)** that of a Be atom in NiBe.

Both NiAl and NiBe have a B2 crystal structure in which each (Al,Be) atom is surrounded by four Ni atoms as shown in Figure 1. The density of NiBe (6.40 g/cm^3) is about 10% more dense than NiAl even though the element beryllium is lighter than aluminum. This density increase is a result of beryllium also being a smaller atom than aluminum which allows the Ni atoms which surround it to pack themselves more closely. The small size of the beryllium atoms would also suggest that they sit more deeply in the well between Ni atoms. Schematics of the relative position of Al and Be atoms in NiBe and NiAl are given in Figure 1b and 1c. The passage of a dislocation would include the movement of a Be atom out of its position and into the next well between Ni atoms. By

sitting more deeply between Ni atoms, the force to move a Be atom in NiBe would seem to be greater and one would predict a greater lattice friction and creep strength in NiBe than in NiAl. The high melting temperature (1605 °C) of NiBe also suggests attractive high temperature creep properties. The specific strength of NiBe may very well be significantly greater than that of NiAl even with its greater density.

This investigation will examine the properties of both polycrystalline NiAl and NiBe at elevated temperatures. Transient tests are performed to determine the dislocation mechanisms which are dominant at various temperatures. The initial results of such tests are presented in the following sections.

Distinction Between Deformation Mechanisms in Transient Tests

Plastic deformation in metals and alloys can be described in terms of two limiting classes: 1) Class I alloys in which the drag forces on the dislocation constrain deformation, and 2) pure metal-type behavior in which the dislocation structure controls deformation.[2] Class I alloys are characterized by solid solution alloys in which solute atoms form an atmosphere around the dislocation core which is dragged along as the dislocation moves. Deformation is controlled, in this case, by the diffusion of this solute atmosphere. In pure metals, on the other hand, dislocation motion is not hindered by solute drag, rather dislocations move into a lower energy regular network. A small percent of dislocations remain mobile but must cut through the network and thus the structure of this network controls the total deformation.

The distinction between Class I and pure metals can be shown clearly by their differing responses in transient tests. A strain rate change test is accomplished by imposing a constant strain rate until steady state deformation occurs and then increasing or decreasing this strain rate as quickly as possible. Figure 2 illustrates the response of both Class I and pure metals during the transient portion of a strain rate change test. A strain rate increase in a Class I alloy must result in an increase in the total number of dislocations which cannot occur instantaneously. Thus Class I alloys seem initially hard in a strain rate increase as the stress initially remains large compared to the steady state stress at the higher rate. Conversely, during a strain rate decrease, Class I alloys appear soft since the dislocation density at the beginning of the decrease is much larger than that at the steady state at the low rate. The transient response of a Class I alloy is controlled by the time needed to multiply dislocations in a strain rate increase and annihilate them during a rate decrease.

The response of pure metals during a strain rate change is distinct from the Class I-type response. In pure metals, most dislocations are stopped but can be made mobile with an increase in stress.

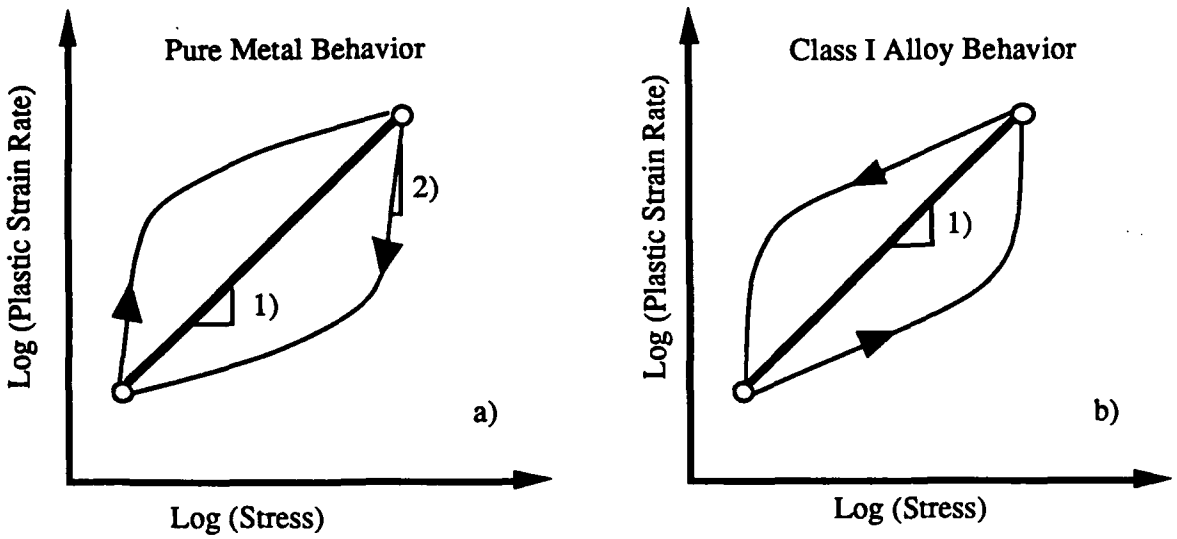

Figure 2. Characteristic responses of **a)** a pure metal and **b)** a Class I alloy during a strain rate change test.

The increase in mobile dislocation density needed in a strain rate increase test is readily available to these alloys with only a small increase in stress and the time for dislocation multiplication is not a limiting factor as with Class I alloys. Thus pure metals seem initially weak in a strain rate increase since many dislocations are available with a small stress increase. This is illustrated in Figure 2a as the ability of a pure metal to reach high strain rates at initially lower stresses than steady state would demand. But at higher strain rates a finer network of immobile dislocations will eventually form producing a harder structure as the new steady state is reached. The hardened structure would persist if the strain rate is decreased until the structure can recover; so that pure metals are characteristically strong in a strain rate decrease transient.

Steady state stress exponents are found in Figure 2 from the slope of the line joining the ending steady states at the high and low strain rates. A constant structure stress exponent is measured during the transient as the initial slope on these plots during a strain rate change.

Strain rate change tests were performed on the intermetallics in this investigation in order to characterize the operative dislocation mechanisms; these results are presented below.

Experimental Procedures

Samples of NiAl and NiBe were provided by the Research and Development Division of the Lockheed Missiles and Space Company. NiAl powders consolidated by heating to 1100 °C and then extruding to a 8 to 1 reduction in a warm press. The grain size of the resulting metal varied

greatly with many grains larger than 100 μm in the extrusion direction. Cylindrical samples were electron discharge machined to diameter of 4.5 mm and 9 mm length. The extrusion direction was positioned as the compression axis for these tests.

Powders of Ni and Be were vacuum induction melted and then chill cast in a graphite mold. The resulting ingot was annealed under vacuum at 1000 °C for 1.5 hours. Cylindrical samples were electron discharged machined from the ingot with a diameter of 4.5mm and a length of 9 mm.

Compression tests were performed in a computer-controlled Instron testing machine under strain rate control. The strain in the sample was measured by a symmetrical LVDT arrangement that measures the displacement of top and bottom ceramic platens which hold the sample. Changes in displacement at the sample of 0.5 μm can be recorded at rates of 20 records per second during the transients of these tests. Constant strain rate tests at 10^{-3} and 10^{-4} s^{-1} were performed as well as strain rate change tests between these rates.

Transient Tests on NiAl

The stress-strain curve of NiAl is shown in Figure 3 for a strain rate increase and strain rate decrease test. The sample shows continued strain hardening throughout the tests so care must be taken to compare tests at the same strain. Even if constant structure is not achieved (strain hardening continues), the change in strain rate is performed at a constant structure and the transient tests are valid. The stress at larger strains (after strain hardening decreases) at strain rates of 10^{-3} and 10^{-4} s^{-1} determined in this investigation are compared with the steady state values measured by Vandervoort, *et al* [3] for Ni - 50.4 Al with a grain size of 1000 μm in Figure 4.

Figure 5 shows the results of the strain rate change tests between 10^{-3} and 10^{-4} s^{-1}. NiAl shows pure metal like behavior as evidenced by both the strain rate increase and strain rate decrease. During a strain rate increase, the intermetallic seems initially soft and moves above the steady state line; during the rate decrease, it appears hard. The constant structure stress exponent is of the order 100 compared with the steady state stress exponent of 6.6. Whittenberger [1] measured a stress exponent of 6.50 for Ni - 49.94 Al at 1300 K.

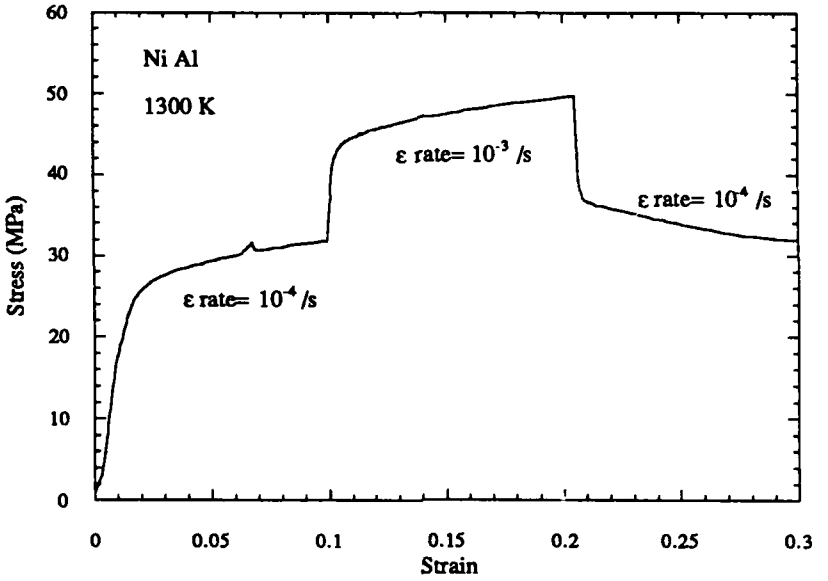

Figure 3. Stress-Strain Curve of NiAl during a strain rate increase and decrease.

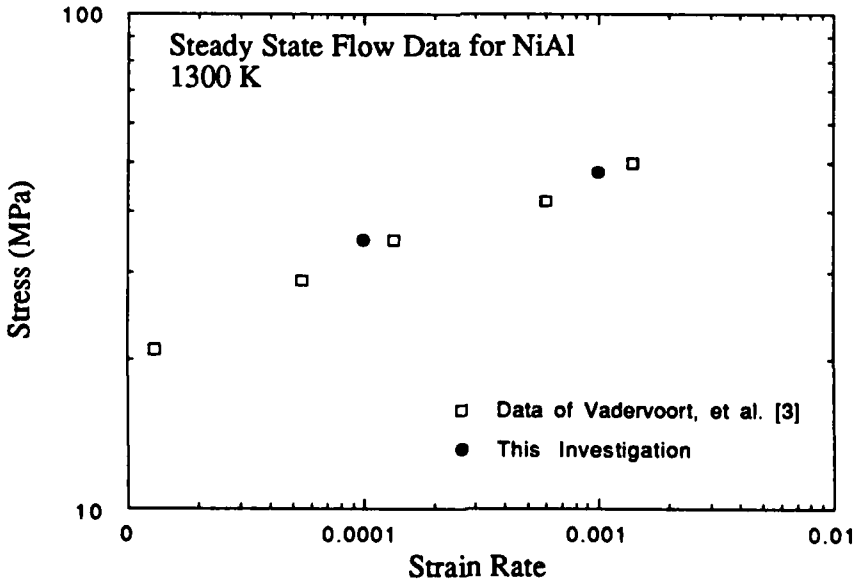

Figure 4. Log(Stress) - Log (Strain Rate) plot for NiAl at 1300 K.

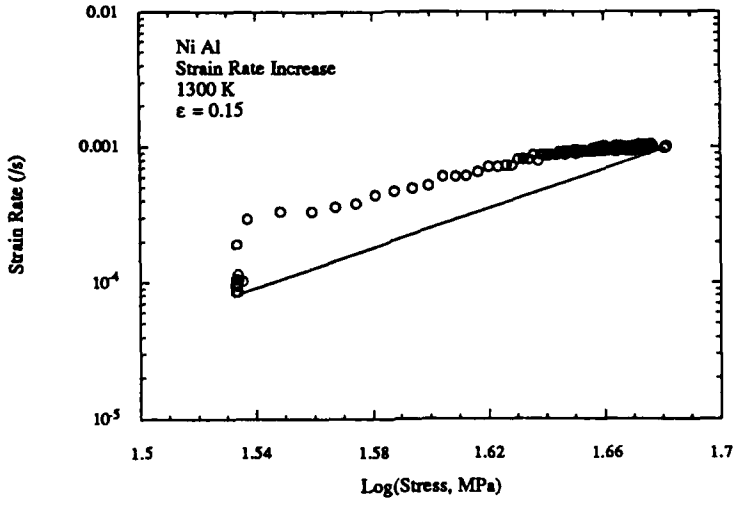

a)

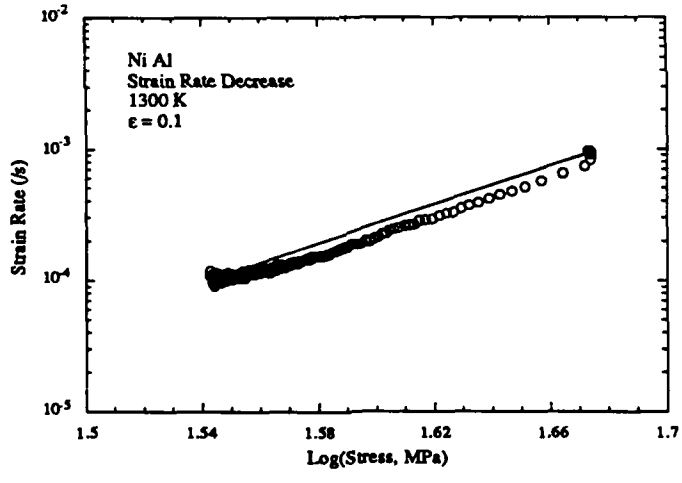

b)

Figure 5. Transient Response of NiAl during **a)** a strain rate increase and **b)** decrease.

Transient Test on NiBe

Strain hardening is also evident in the stress-strain curve of cast NiBe in Figure 6. The flow stress of NiBe is also found to be about 2.5 greater than NiAl at 1300 K. The flow stress of NiBe as shown in Figure 7 does not decrease rapidly with temperatures dropping to only 60 MPa at 1400 K.

Strain rate change tests reveal the pure metal behavior of NiBe at both 1300 K and 1400 K (Figures 8 and 9). The stress exponent of NiBe is found to be 5.7 at 1300 K and 5.0 at 1400 K.

The constant structure stress exponent at these temperatures is of the order 250.

Conclusions

Strain rate change tests on NiAl and NiBe reveal that deformation is controlled in these intermetallics by dislocation structure and not dislocation mobility. Dislocation structure was also determined important in Ni_3Al as reported in Section B. The high temperature strength of NiBe was found to be more than twice that of NiAl with only a 10% increase in density. Thus, the specific strength of NiBe is superior to that of NiAl though both are limited by brittleness at low temperatures. Further research will concentrate on defining more accurately the role of dislocation structure through additional transient tests.

References

1. J. D. Whittenberger, *J. Mater. Sci.* **22**, 394 (1987).
2. D. L. Yaney, J. C. Gibeling and W. D. Nix, *Acta Metall.* **35**, 1391 (1987).
3. R. R. Vandervoort, A. K. Mukherjee and J. E. Dorn, *Acta Metall.* **59**, 930 (1966).
4. G. M. Pharr and T. G. Nieh, unpublished data.

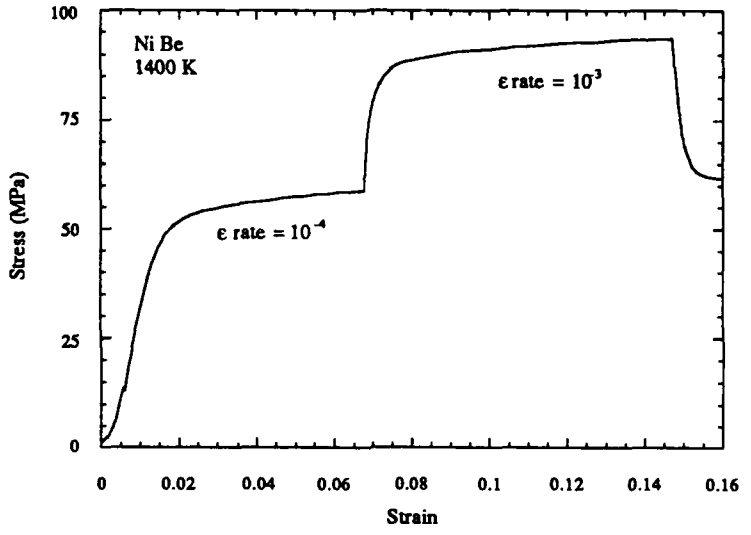

Figure 6. Stress-Strain Curve of NiBe during a strain rate increase and decrease.

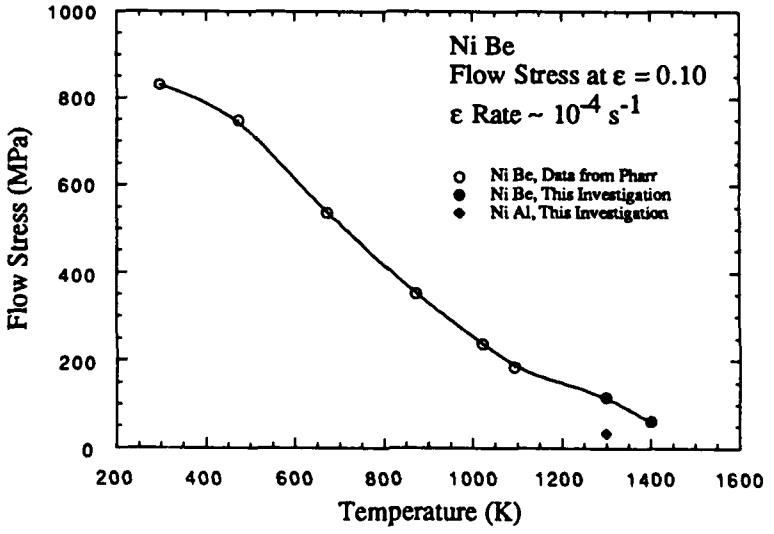

Figure 7. Flow Stress of NiBe as a function of temperature. Data below 1200 K is from Pharr [4]. The flow stress of NiAl at 1300 K is provided for comparison.

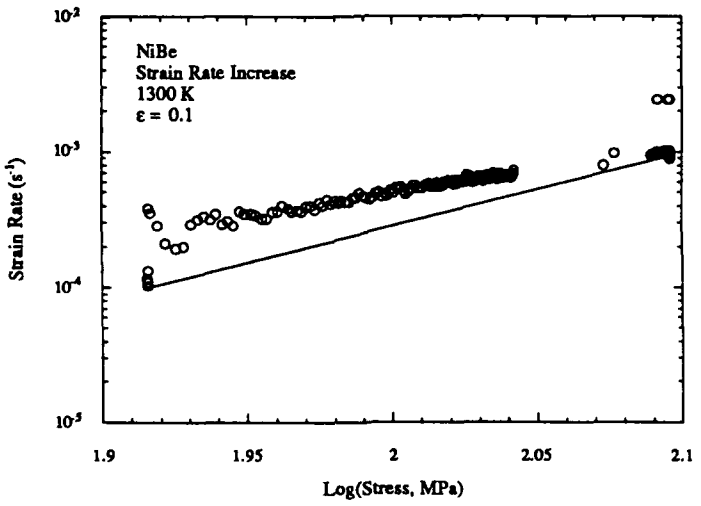

a)

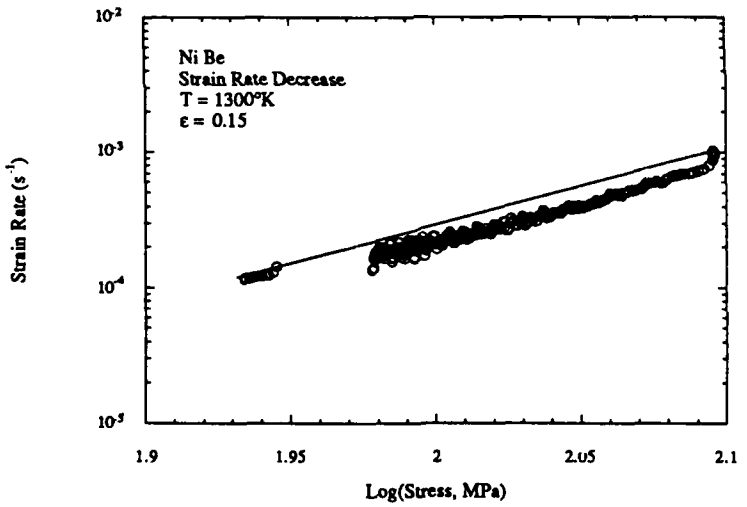

b)

Figure 8. Transient response of NiBe during **a)** a strain rate increase and **b)** decrease at 1300 K.

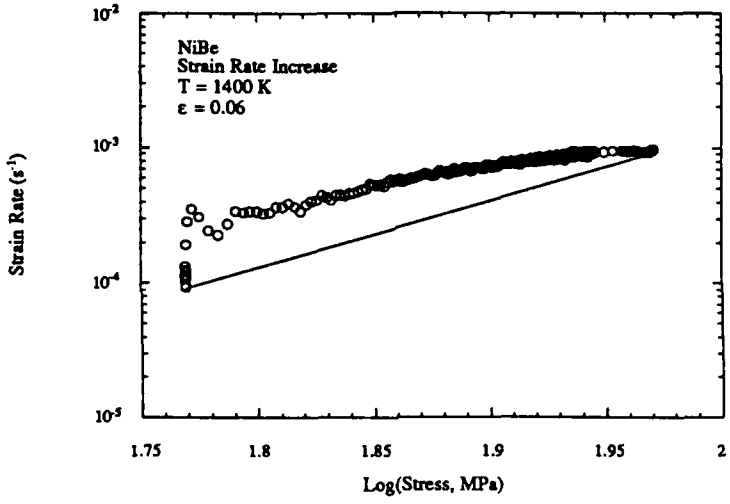

a)

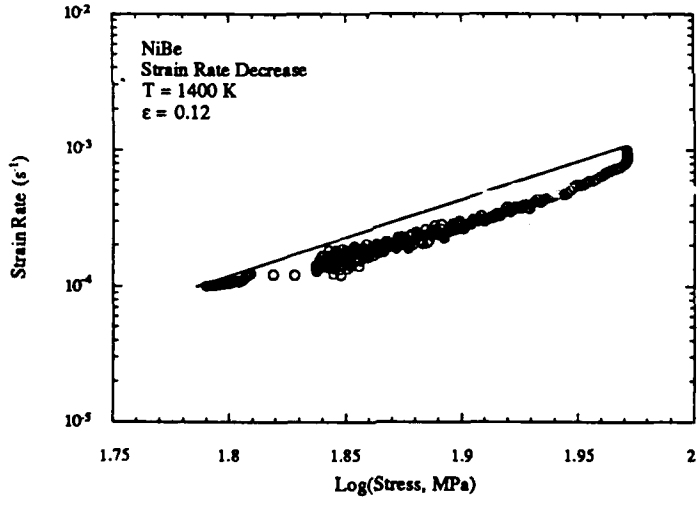

b)

Figure 9. Transient response of NiBe during **a)** a strain rate increase and **b)** decrease at 1400 K.

E. A Model of Dislocation Structure Control of Plastic Deformation

K. R. Forbes (Graduate Research Assistant)

Transient tests with intermetallic alloys suggests that pure metal alloy behavior is the best description of plastic flow in these metals and that dislocation sub-structure controls deformation. For this reason we have concentrated on developing a model that is consistent with deformation in pure metals. The dislocation mechanisms in intermetallic alloys are not known with certainty though various theories have been proposed. Our approach has been to concentrate on a much better characterized metal, copper, in order to develop the model and then to correlate the basics of the model with suggested dislocation mechanisms in intermetallic alloys. The model in this investigation is derived from that of Pharr and Nix [1]. Transient tests can be run with this model and used to reproduce the transient responses of pure metals. From such simulations, the pure metal characteristics described in the previous section can be understood in terms of the mechanisms operational in the model.

Dislocations in copper are known to form tangled arrays in which each dislocation is pinned at various points along its length by interactions with other dislocations. A distribution of free lengths between pinning points exists for the total dislocation density. Although the total dislocation density will increase with plastic strain as dislocations move through the sample and multiply, there is a distribution of dislocation lengths between pinning points. The mathematical form of this distribution of dislocation lengths has been assumed constant in this model which has been shown to be a good approximation for dislocations in copper. At a given stress only those free lengths longer than some critical length will bow out and become mobile while the majority of the dislocation lengths are too small and remain sessile. Thus the mobile dislocation density can be calculated as the integral of the distribution of free lengths which are greater than the critical length defined by the local stress. The local stress, the accumulated plastic strain and the form of the distribution of dislocation lengths are sufficient to calculate the mobile dislocation density in this model.

The stress applied to the crystal is not, in general, the local stress at the dislocation which drives the free lengths. The long range backstress of the dislocation network must be subtracted from the total stress in order to determine the local stress. The backstress is assumed to have a square root dependence on the total dislocation density. Such an approach results in a relatively simple relation of the mobile dislocation density which can be described as a function of only the applied stress and accumulated plastic strain.

$$\rho_{mob} = f\left[\sigma_{app}, \varepsilon_{pl}\right] \qquad 1)$$

The velocity of dislocations in copper is only a weak function of the local stress. The model uses a linear dependence of the velocity on stress for copper which reproduces the known dependence of dislocation velocity quite well. Since the local stress depends on the applied stress and the total dislocation density, the dislocation velocity is a function of both stress and plastic strain.

$$v = f\left[\sigma_{app}, \varepsilon_{pl}\right] \qquad 2)$$

The Orowan relation equates the plastic strain rate in any metal to the product of the mobile dislocation density, the dislocation velocity and the Burgers vector, b of the dislocation. Since we have derived analytical expressions for the mobile dislocation density and velocity, the equation for the plastic strain rate is straightforward.

$$\dot{\varepsilon}_{pl} = \rho_{mob} \cdot b \cdot v$$

$$\dot{\varepsilon}_{pl} = f\left[\sigma_{app}, \varepsilon_{pl}\right] \qquad 3)$$

The form of equation (3) is identical to that of Pharr [1]. The simulations with this model are performed for constant total strain rate, which is the sum of the plastic strain rate in equation (3) and the elastic strain rate. The elastic strain which was ignored by Pharr is included here in order to model transient tests.

$$\varepsilon_{tot} = \varepsilon_{pl} + \varepsilon_{el}$$

$$\varepsilon_{tot} = \varepsilon_{pl} + \frac{\sigma}{E} \qquad 4)$$

The model uses a simple forward Euler technique to advance along in time for a simulated tests. Calculations were repeated at smaller time steps to confirm the convergence of these solutions. For a constant strain rate, the plastic strain at the beginning of the time step is used in equation (4) to determine the new applied stress. The new stress and plastic strain determine the current plastic strain rate in equation (3). For a given time step, this plastic strain rate can be used to compute the new plastic strain and then the process is repeated. The model was run with the appropriate constants for copper at a strain rate of 10^{-4} s^{-1} and the results compared with the experiments of Carraker and Hibbard [2] in Figure 1. Since the model only allows for dislocation multiplication

with strain and not for any dynamic recovery, it is expected that the results will diverge at very large strains.

For a stress relaxation simulation, the total strain in equation (4) is set constant after an initial strain of 0.10 is reached. The resulting relaxation is shown in Figure 2 along with a log-log plot of the plastic strain rate with stress to reveal the stress sensitivity of the relaxation. The stress sensitivity is 325 which is comparable with experimental reports of stress sensitivity in copper. Figure 3 reveals how the dislocation structure changes during the course of a stress relaxation. Although the dislocation velocity remains constant during the relaxation, the mobile dislocation density drops rapidly until the strain rate is unmeasurable. Thus the limiting process in the relaxation of copper is not the velocity of the dislocations but rather their rapid immobilization. As the stress decreases, the critical length of free dislocation increases until there is a minimal distribution of free length large enough to move. In this way, all of the dislocations in the sample are rapidly immobilized during a stress relaxation.

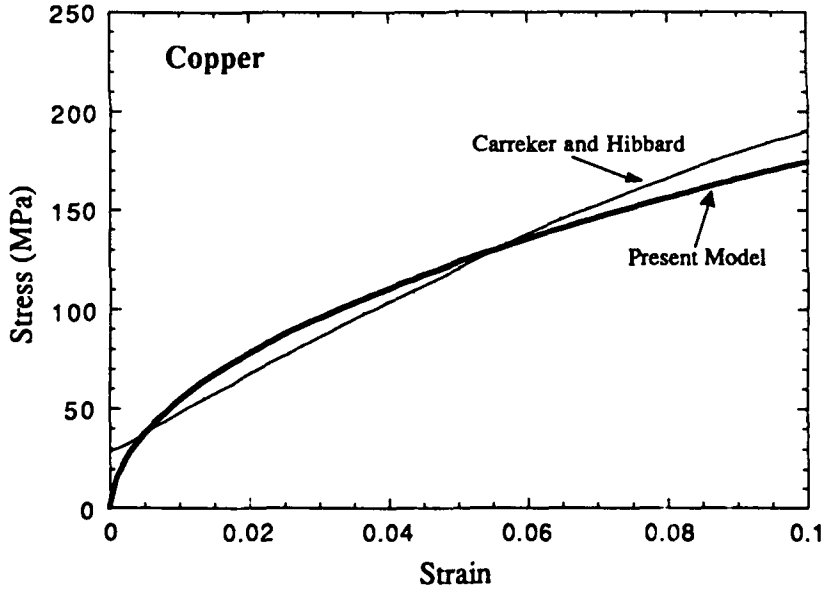

Figure 1. A comparison of the stress-strain prediction of this model (ε rate = 10×10^{-4} s^{-1}) for copper with the experimental data of Carraker and Hibbard [2] (T = 300 K, ε rate = 6×10^{-4} s^{-1}, 0.090 mm grain size).

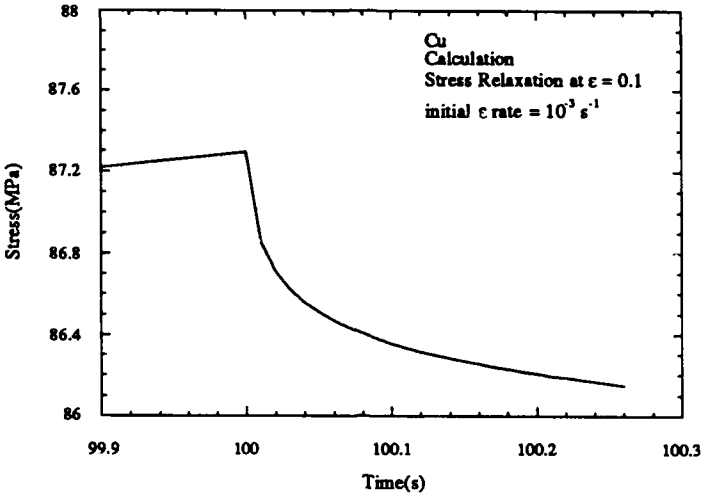

a)

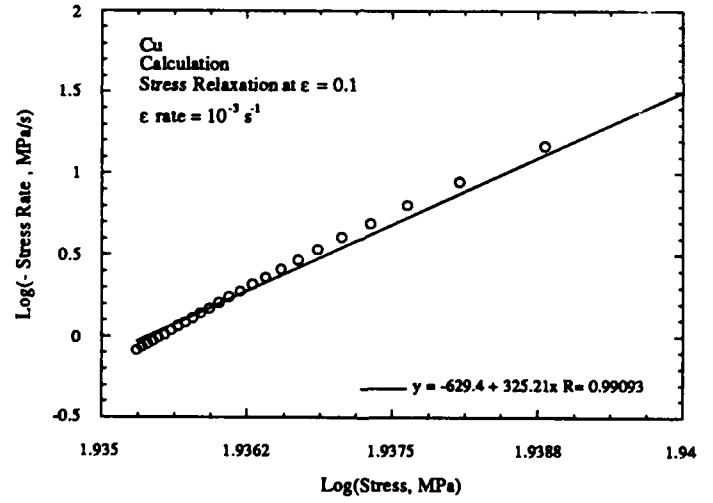

b)

Figure 2. **a)** The stress relaxation of copper at low temperatures as calculated by this model. Relaxation begins at time = 100 s. **b)** A plot of log(Stress) vs. log(- Stress Rate)for this relaxation revealing the large stress exponent derived from these calculations.

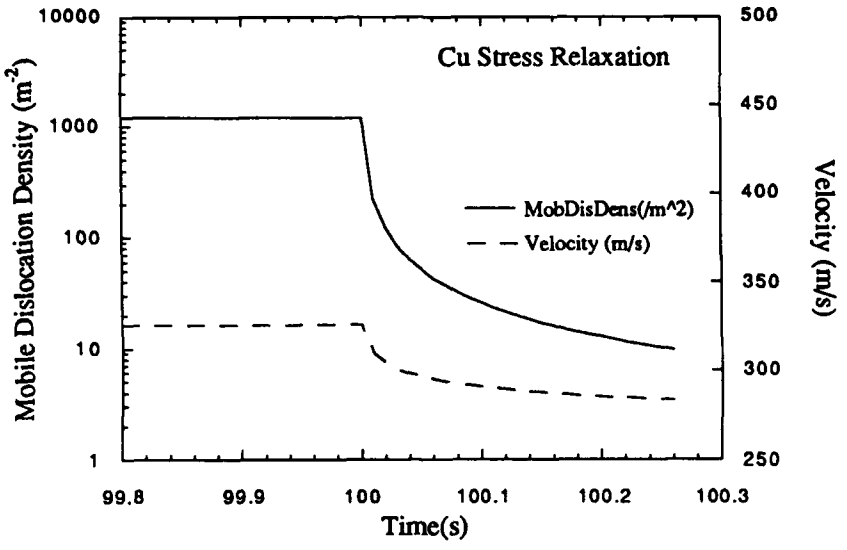

Figure 3. The evolution of the mobile dislocation density and the dislocation velocity during a stress relaxation.

If deformation were mobility controlled, the relaxation rate would be an exponential function of the stress. Mobility controlled deformation would thus produce a linear relationship on a log(stress) vs. stress plot and a logarithmic decay of the stress with time. In figure 4, these plots are shown and clearly illustrate that dislocation mobility control is not predicted by this model.

The model of this investigation shows rapid dislocation immobilization limiting stress relaxation in copper. The intermetallic, Ni3Al has a stress relaxation response similar to copper and a large stress exponent suggesting dislocation structure control. The basis of dislocation immobilization is very different in copper and Ni3Al. Whereas the free dislocation lengths are defined in copper as the distance between pinning points of a given distribution in the dislocation network, free lengths in Ni3Al are determined by distances between Kear-Wilsdorf locks as described in Section C. The pinning of dislocations with Kear-Wilsdorf locks is a stochastic process and currently no such process exists in the model. Dislocation lengths could conceivably be tracked in time and probabilities of pinning could determine the evolution of the structure in Ni3Al but only with a large increase in computational difficulty. Nonetheless, a general comparison between this model and tests in Ni3Al supports dislocation immobilization as the limiting process for stress relaxation in Ni3Al.

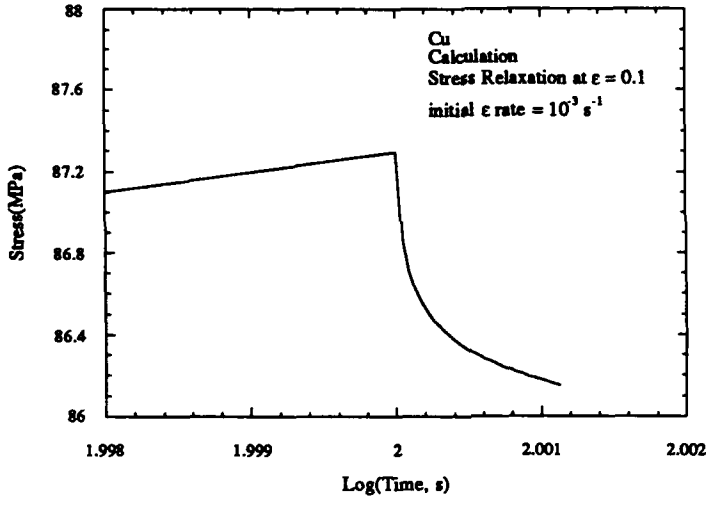

a)

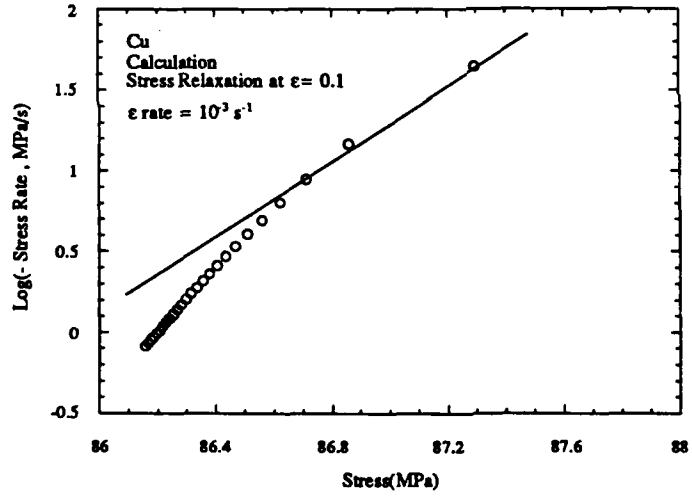

b)

Figure 4. **a)** The stress vs. log(time) plot of a stress relaxation calculation for copper. **b)** A plot of log(- Stress Rate) vs. stress plot for this relaxation. Neither plot is consistent with mobility controlled deformation.

References

1. G. M. Pharr and W. D. Nix, *Acta Metall.* **27**, 433 (1979).
2. R. P. Carraker, Jr. and W. R. Hibbard, Jr, *Acta Metall.* **1**, 654 (1953).

III. ORAL PRESENTATIONS RESULTING FROM AFOSR GRANT NO. 89-0201

1. W.D. Nix, ""Advances in Understanding High Temperature Strengthening of Metals and Alloys", 1989 Edward deMille Campbell Memorial Lecture, Annual Meeting of ASM International, Indianapolis, Indiana, October 3, 1989.

2. K.J. Hemker and W.D. Nix, "Intermediate and High Temperature Creep Properties of Ni3Al Single Crystals", Symposium on High Temperature Aluminides and Intermetallics, Fall Meeting of the Metallurgical Society, Indianapolis, Indiana, October 2, 1989.

3. K.J. Hemker, M.J. Mills and W.D. Nix, "A Critical Analysis of the Dislocation Mechanisms Associated with Yielding in Ni3Al, Poster Session on High Temperature Aluminides and Intermetallics, Fall Meeting of the Metallurgical Society, Indianapolis, Indiana, October 3, 1989.

4. K.J. Hemker and W.D. Nix, "An Investigation of Creep in Ni3Al(B,Hf)", Fourth International Conference on Creep and Fracture of Engineering Materials and Structures, Swansea, Wales, April 2-6, 1990.

IV. PUBLICATIONS RESULTING FROM AFOSR GRANT NO. 89-0201

1. K.J. Hemker and W.D. Nix, "An Investigation of Creep in Ni3Al(B,Hf)", Proceedings of the Fourth International Conference on Creep and Fracture of Engineering Materials and Structures, Swansea, Wales, Eds: B. Wilshire and R.W. Evans, The Institute of Metals, (1990), p.51.

2. C.-M. Kuo, K.R. Forbes, S.P. Baker and W.D. Nix, "On the Question of Strain Rate Continuity in Stress Rate Change Experiments", Scripta Metall., 24, 1623-1628 (1990).

3. K.J. Hemker, M.J. Mills and W.D. Nix, "An investigation of the Mechanisms that Control Intermediate Temperature Creep of Ni3Al", (accepted for publication in Acta Metall.)

4. K.J. Hemker, M.J. Mills, K.R. Forbes, D.D. Sternbergh and W.D. Nix, "Transient Deformation in the Intermetallic Alloy, Ni3Al" (to be published in Proceedings of the ASM Symposium on Modelling the Deformation of Crystalline Solids: Physical Theory, Application, and Experimental Comparisons, 1991)